Comprehensive Summaries of Uppsala Dissertations
from the Faculty of Science and Technology 683

Design and Stability of $Cu(In,Ga)Se_2$-Based Solar Cell Modules

BY

JOHAN WENNERBERG

ACTA UNIVERSITATIS UPSALIENSIS
UPPSALA 2002

Dissertation for the Degree of Doctor of Philosophy in Solid State Electronics presented at Uppsala University in 2002

ABSTRACT

Wennerberg, J. 2002. Design and Stability of Cu(In,Ga)Se_2-Based Solar Cell Modules. Acta Universitatis Upsaliensis. *Comprehensive Summaries of Uppsala Dissertations from the Faculty of Science and Technology* 683. 91 pp. Uppsala.
ISBN 91-554-5214-0

Cu(In,Ga)Se_2 (CIGS) is one of the most promising semiconductor compounds for large-scale production of efficient, low-cost thin film solar cells, and several research institutes have announced their plans for CIGS production lines. But for the CIGS technology to become a commercial success, a number of issues concerning manufacturability, product definition, and long-term stability require further attention.

Several studies indicate that CIGS-based modules are stable over many years in field operation. At the same time, it is shown in the present work that they may have difficulties in passing standard accelerated lifetime test procedures like the IEC 1646 damp heat test. In particular, CIGS modules are sensitive to humidity penetrating through the module encapsulation, which will increase the resistive losses in the front contact and cause severe corrosion of the back contact. It is also shown that cells experience degradation in both voltage and fill factor, and the causes of these effects are addressed.

By concentrating the light falling onto a solar cell, the device will deliver a higher power output per illuminated absorber area, which can lower the electricity production costs. For CIGS-based solar cells, low-concentrated illumination could be an economically viable approach. In this work it is shown that the yearly performance of a photovoltaic system with CIGS modules can be significantly improved at a moderate cost by using parabolic aluminum mirrors as concentrating elements. However, in order to avoid detrimental power losses due to high temperatures and current densities, the modules need to be designed for the higher light intensity and to be sufficiently cooled during operation. A design where the front contact of the module is assisted by a metal grid has shown promising results, not only for concentrated illumination but also for normal operation. The benefits are enhanced window processing tolerance and throughput, as well as improved degrees of freedom of the module geometry.

Johan Wennerberg, Ångström Solar Center, Uppsala University
P. O. Box 534, SE-751 21 Uppsala, Sweden

ISSN 1104-232X
ISBN 91-554-5214-0

Printed in Sweden by Reklam & Katalogtryck, Uppsala 2002

Publications

This thesis is based on the following publications, which will be referred to in the text by their Roman numerals.

I J. Wennerberg, J. Kessler, M. Bodegård, and L. Stolt, *Damp Heat Testing of High Performance CIGS Thin Film Solar Cells*, in proceedings 2nd World Conference on Photovoltaic Solar Energy Conversion (1998) 1161–1164.

II J. Kessler, J. Norling, O. Lundberg, J. Wennerberg, and L. Stolt, *Optimization of RF-Sputtered ZnO/ZnO:Al for Cu(In,Ga)Se_2 Based Devices*, in proceedings 16th European Photovoltaic Solar Energy Conference (2000) 775–778

III J. Wennerberg, J. Kessler, and L. Stolt, *Degradation Mechanisms of Cu(In,Ga)Se_2 Thin Film PV Modules*, in proceedings 16th European Photovoltaic Solar Energy Conference (2000) 309–312

IV J. Wennerberg, J. Kessler, and L. Stolt, *Design of Grided Cu(In,Ga)Se_2 Thin Film PV Modules*, Solar Energy Materials & Solar Cells **67** (2001) 59–65

V J. Wennerberg, J. Kessler, J. Hedström, L. Stolt, B. Karlsson, and M. Rönnelid, *CIGS Thin Film PV Modules for Low-Concentrating Systems*, Solar Energy **69** (2001) 243–255

VI M. Brogren, J. Wennerberg, R. Kapper, and B. Karlsson, *Design of Concentrating Elements with Thin Film Solar Cells for Wall Integration*, Solar Energy Materials & Solar Cells (in press)

VII J. Kessler, J. Wennerberg, M. Bodegård, and L. Stolt, *High Efficient Cu(In,Ga)Se_2 Mini-Modules*, Solar Energy Materials & Solar Cells (in press)

VIII J. Wennerberg, J. Kessler, and L. Stolt, *Cu(In,Ga)Se_2-Based Modules Optimized for Long-Term Performance*, Solar Energy Materials & Solar Cells (in press)

Related work

The following publications are the outcome of research work outside the scope of this thesis.

i M. Rönnelid, B. Karlsson, P. Krohn, and J. Wennerberg, *Booster Reflectors for PV Modules in Sweden*, Progress in Photovoltaics: Research and Applications **8** (2000) 279–291

ii M. Igalson, M. Wimbor, and J. Wennerberg, *The Change of the Electronic Properties of CIGS Devices Induced by "Damp Heat" Treatment*, Thin Solid Films (in press)

iii J. Malmström, J. Wennerberg, and L. Stolt, *Influence of Ga on the Current Transport in Cu(In,Ga)Se_2 Thin Film Solar Cells*, in proceedings 17th European Photovoltaic Solar Energy Conference (2001)

iv J. Kessler, M. Bodegård, J. Hedström, J. Wennerberg, J. Norling, and L. Stolt, *Cu(In,Ga)Se_2 Devices: From Cells to Mini-Modules*, presented to the E-MRS 2000 Spring Meeting (2000)

v G. A. Medvedkin and J. Wennerberg, *Laser Beam Induced Current Characterization of High Efficiency CIS and CIGS Solar Cells*, Thin Films and Devices **67**–**68** (1999) 69–74

vi G. A. Medvedkin, L. Stolt, and J. Wennerberg, *Laser Scanning Obtained Optoelectronic Images of Polycrystalline Thin Film Solar Cells based on $CuInSe_2$ and Cu(In,Ga)Se_2*, Semiconductors **33** (1999) and Fizika i Tekhnika Poluprovodnikov **33** (1999)

vii G. A. Medvedkin and J. Wennerberg, *Computer Modeling and Visualization of Hidden Defects in Thin Film Solar Cells With CdS, $CuInSe_2$ and Cu(In,Ga)Se_2 Layers* (in manuscript)

viii J. Wennerberg and L. Stolt, *Technical and Physical Requirements on Solar Cells for Concentrating Systems* (in Swedish), Ångström Solar Center report ÅSC-011-CIGS-98 (1998)

ix J. Wennerberg, and L. Stolt, *Performance Analysis of Standard Crystalline Silicon Solar Cells in Low-Concentrated Light*, internal PM within the framework of ELFORSK Projekt 2080 – SOLEL 97-99, Ångström Solar Center (1998)

Contents

1 Introduction to photovoltaics

If there is a dream solar technology, it is photovoltaics – the direct conversion of sunlight into electricity by solar cells. It is the most sophisticated solar energy technology and, at the same time, one of the simplest, most environmentally benign sources of electricity yet conceived. Photovoltaic devices, or solar cells, use semiconductor materials to directly convert sunlight into electricity without any noise or pollution. Solar cells have no moving parts – power is produced when sunlight strikes the semiconductor material and creates electric voltage and current.

Solar cells are traditionally used to power remote residences, satellites, highway signs, water pumps, communication stations, navigation buoys, streetlights and calculators, but as new photovoltaic materials and technologies emerge, the interest for using photovoltaics for large-scale power production is growing.

There is a strong need to develop renewable energy resources. Today, nearly 80% of all energy used worldwide originate from fossil fuels like coal, oil and natural gas [1]. This massive exploitation of fossil fuels imposes a major threat to the environment in terms of emission of greenhouse gases and acid rain. In a business-as-usual scenario, the global energy demand is projected to grow by close to 60% and CO_2 emissions by 70% from 1997 to 2020 [2]. Two thirds of this increase is directly related to improved living standards in developing countries [3] where the main drivers include rapid economic growth and industrial expansion, and high rates of population increase and urbanization. Despite the increasing energy demand, there seem to be no physical limits to the world's energy supply for at least the next 50 years [4]. Nevertheless, today's energy system is unsustainable because of equity issues as well as environmental, economic, and geopolitical concerns that have implications far into the future. Modern fuels and electricity are not universally accessible – an inequity that has moral, political, and practical dimensions in a world that is becoming increasingly interconnected. Furthermore, the current energy system is not sufficiently reliable or affordable to support widespread economic growth. The productivity of one-third of the world's population is compromised by lack of access to commercial energy, and perhaps another third suffer economic hardship and insecurity due to unreliable energy supplies. In addition, the negative local, regional, and global environmental impacts of energy production and use, threaten the health and well-being of current and future generations.

The photovoltaic technology has the potential to give a substantial input to the energy supply in the future, and to be part of creating a sustainable energy system. But lowering the cost of power production to the point at which solar is competitive with other options is critical if solar power is ever to become a core generation technology.

1.1 Solar power

The sun is a spherical source of about 1.39 million km diameter, at an average distance of 149.6 million km from earth. Radiation from the sun sustains life on earth and determines the climate. The energy flow within the sun results in a surface temperature of around 5800 K, and the spectrum of the radiation from the sun is therefore similar to that of a 5800 K blackbody. The amount of solar energy received per unit of time and per unit area on a surface normal to the sun just outside earth's atmosphere, is called the solar constant. Measuring the value of the

solar constant was an important task for researchers during the 19th century. One of the most outstanding scientists in this field was Knut Ångström, who developed a modified pyrheliometer that was accepted as the standard instrument for measuring solar irradiation at the 1905 Solar Congress in Oxford [5]. A modern value of the solar constant is 1353±21 W/m^2 [6] where the differential is caused by variations in solar activity as well as changes in the distance of the earth from the sun due to a small ellipticity of the earth's orbit.

Figure 1 shows the spectrum of the solar radiation outside the earth's atmosphere. The range 200–2500 nm includes 96.3% of the total irradiance. The solar constant is the total integrated irradiance over the extraterrestrial spectrum, plus the additional 3.7% from wavelengths outside this interval. The spectrum of the solar radiation at the earth's surface has several components. The direct portion of the radiation is collimated within an angle of about 0.53°, while the diffuse portion is incident from the hemispheric sky and scattered from the surroundings. The total ground radiation, i.e. the sum of all components, is called the global radiation.

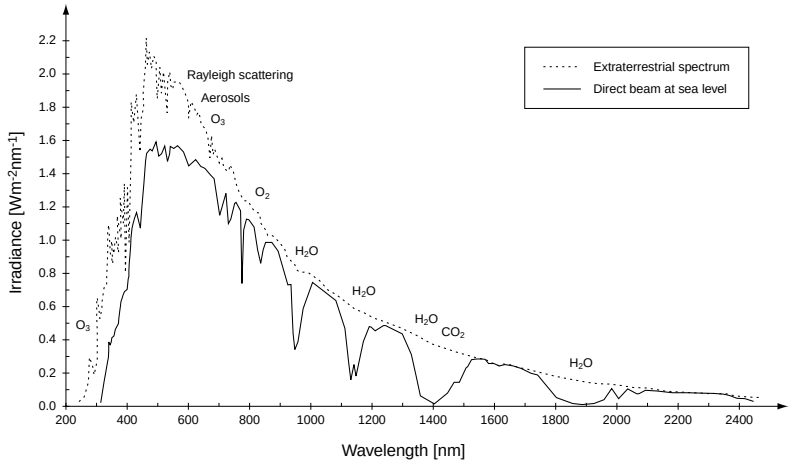

Figure 1. Extraterrestrial and direct sea level solar irradiation spectrums. After [7].

All radiation that reaches ground passes through the atmosphere, which modifies the spectrum by absorption and scattering. Atomic and molecular oxygen and nitrogen absorb very short-wave radiation, effectively blocking radiation at wavelengths below 190 nm. Splitting of oxygen molecules induces production of ozone that strongly absorbs at longer wavelengths. Water vapor, carbon dioxide and oxygen, selectively absorb in the near infrared. Wavelength dependent Rayleigh scattering and scattering from particulates containing water droplets, so called aerosols, changes the spectrum and makes the sky blue. For a typical cloudless atmosphere and zero zenith angle, the irradiance reaching the outer atmosphere is reduced to approximately 1050 W/m^2 direct beam radiation, or 1120 W/m^2 global irradiation, on a horizontal surface at sea level [7].

Seen annually, insolation varies over the earth's surface by a factor of 3, from roughly 800 kWh/m^2·year in northern Scandinavia and Canada to a maximum of 2500 kWh/m^2·year in some dry desert areas. The differences in average monthly insolation can vary from 25% close to the equator to a factor of 10 in very northern

and southern areas [4]. The total average power available at the earth's surface in the form of solar radiation exceeds the total human power consumption by roughly a factor of 1500 [4]. Calculated per person, the average solar power available is 3 MW, while the average power use varies from 100 W in the least industrialized countries to 10 kW in the USA. Although these numbers provide a rough picture of the absolute boundaries of the global potential of solar energy, they have little significance for the technical and economic potential, which is regionally dependent upon differences in the solar energy supply, energy infrastructure, population density, geographic conditions, financing schemes, and, not least, political structures.

In the following subsections, some key technologies for harnessing the power from the sun are briefly reviewed. Photovoltaics will be further discussed in following chapters, but since solar heating and the other solar energy technologies are beyond the scope of this thesis the reader is referred to basic textbooks on solar energy and applications for additional information.

1.1.1 Solar heating

The easiest and most direct application of solar energy is the direct conversion of sunlight into low-temperature heat (up to 100 °C). In general, two classes of technologies can be distinguished, namely passive and active solar energy conversion. Active conversion relies on a solar collector, and the heat is transported to the process by a medium, often water. For passive systems, the conversion takes place in the process, so no active components are used. The best-known technology for active solar heating is the solar domestic hot water systems. Another technology in the building sector is solar space heating system. Such a system can be sized for single houses or for collective buildings and district heating. Similar technologies can be applied in the industrial and agricultural sector for low-temperature heating and drying applications. Heating using solar energy can also be achieved by heat pumps. Finally, there are technologies to use thermal solar for cooling and cooking purposes.

1.1.2 Photovoltaics

Photovoltaic solar energy conversion is the direct conversion of sunlight into electricity. This can be done by flat plate or concentrator systems. An essential component of these systems is the solar cell, in which the photovoltaic effect takes place. The photovoltaic effect is the generation of free electrons and an electric current by using the energy of light. Today's commercially available photovoltaic devices are fabricated from semi-conducting materials. The most commonly used material is silicon, to which small amounts of impurities, typically boron and phosphorous, are added. In this process, which is called doping, one region with excess of free electrons (called *n*-type) and one region with excess of holes (called *p*-type) are created. In the junction between these regions (the *p*-*n* junction) a static internal electric field is formed. This field, which is directed from the *n*-type region towards the *p*-type region, separates the electrons and holes that are produced when the material is illuminated. At wavelengths where the photons have energies above a certain threshold energy (the bandgap energy) the light will be absorbed in the semiconductor material and an electron-hole pair is created. If the electron-hole pair is generated close enough to the *p*-*n* junction the carriers can be separated by the internal electrical field and contribute to the generated current.

The efficiency of the conversion from sunlight to electricity in a photovoltaic solar power system is typically 10–15%. Hence, substantial areas are required to capture and convert significant amounts of solar energy to fulfill the energy needs relative to today's energy use. For instance, at a plant efficiency of 10%, an area of 3–10 km^2 is required to generate an average power of 100 MW, resulting in a yearly electricity generation of 0.9 TWh [4]. Some of the more provocative solar energy experts, however, claim that this is not a problem – there are desert areas more than enough to supply the world with solar electricity. Covering an area of 500 000 km^2, corresponding to approximately 5% of the Sahara desert, with 10% efficient solar panels would provide sufficient amounts of electricity to meet the total global energy needs [8]. In this scenario, photovoltaic systems would be placed in many desert areas around the world and connected in a worldwide solar energy grid.

In densely populated countries with a well-developed infrastructure, there is an emphasis on applications of grid-connected photovoltaic systems in the built environment. These systems are necessarily small or medium sized, typically between 1 kW and 1 MW. The electricity is generated close to the place where electricity is also consumed. In less densely populated countries there is a considerable interest in ground-based power plants, generally larger than 1 MW. In countries or rural regions with a weak grid infrastructure, small standalone systems and modular electric systems may be used for electrification of houses or village communities. Grid connected systems here account for only a small fraction, while the majority are small standalone systems used for water pumping, communication, leisure, consumer products, etc.

1.1.3 Solar thermal electricity

Solar radiation can produce high-temperature heat, which can be used to generate electricity. The most important solar thermal electricity technologies use concentrators and thus direct irradiation. Low cloud areas with little scattered radiation, such as deserts, are considered most suitable for this technology. The collector captures and concentrates solar radiation, which is then delivered to the receiver. The receiver absorbs the concentrated sunlight, transferring its heat energy to a working fluid. The transport and storage system passes the fluid from the receiver to the power conversion system, where a generator running on a thermodynamic cycle generates electricity. An inherent advantage of solar thermal electricity technologies is their ability to be integrated with conventional thermal plants in parallel with a fossil-fuelled boiler. The primary market for concentrating solar thermal electric technologies is in warm sub-tropical, or desert areas, where the fraction of diffuse radiation is low. About 1% of the world's desert area used by solar thermal power plants would be sufficient to generate the total global electricity demand [4].

1.1.4 Space electricity

A very different approach to exploiting solar energy is to capture it in space and convey it to the earth by wireless transmission. In space the maximum irradiance is higher than on earth and is nearly constant. Unlike terrestrial capture of solar energy, a space-based system would not be limited by the weather or the day-night cycle, and so could provide base load electricity 24 hours a day [9]. This energy can be captured and converted to electricity by satellites in geosynchronous orbits designed as large solar collectors. The generated electricity is transformed into

radio frequency form and transmitted by antennas down to earth, where receiving antennas collects the incoming radio frequency energy and convert it into electricity again. The power yield from these antennas would be in the order of 30 MW per km^2 [4]. As with any solar source, space-based energy would not contribute to greenhouse gas emissions during operation. However, launching the systems into space could affect the earth's atmosphere. The effects of power transmission to the ground need to be assessed for at least three factors: influences on the atmosphere, inference between the wireless power transmission and communications or electronic equipment, and the effects of the transmitted beam on life forms.

1.2 Development of photovoltaics

Photovoltaics may be considered somewhat of a space-age technology, but it is a technology that in fact has been around for quite some time. The photovoltaic effect was first reported in 1839 by the French physicist Edmond Becquerel. Like so many of his colleagues of that period, he devoted much time to the study of electricity. In one of a series of electrical experiments, he placed two metal plates in a conductive fluid, and when he by accident exposed the setup to the sun he observed a small voltage. Almost 40 years later, in 1877, the Englishman Willoughby Smith discovered that selenium was sensitive to light. His findings stimulated the scientist William Adams and his student Richard Day to conduct further tests with selenium. Their work demonstrated that when light struck selenium, an electrical current was generated. Having seen the industrial potential of Adams' and Day's work, the American Charles Fritts carried on his own experiments with selenium and developed the first selenium solar cell in 1886. The device had less than 1% conversion efficiency, but nevertheless, Fritts realized the importance of his discovery, and in an early publication he expressed that one of the great advantages with solar cells is that *"the supply of solar energy is both without limit and without cost, and will continue to stream down on earth after we exhaust our supplies of fossil fuels"*. In today's world it is still true that the supply of solar energy is immense. However, during the more than one hundred years that have passed since Charles Fritts foresaw free energy for everyone, we have learnt that the technology for harnessing solar power neither is without limits nor without cost.

The foundation for the modern solar cell technology was built in the 1950s by scientists at the American Bell Telephone Laboratories. Daryl Chapin and his research team were investigating ways to improve the performance of selenium cells as a reliable alternative power source for communication systems in remote areas. At the same time, another Bell scientist, Calvin Fuller, was researching ways of making silicon a better rectifier. Fuller found that silicon worked more efficiently when doped with certain impurities. More or less by chance, Fuller's co-worker Gerald Pearson put the impure silicon under a lamp and measured a rather large amount of electrical current. The silicon solar cell was born. With joint efforts, the two research teams refined the solar cell, and could after a few months present a cell with 6% conversion efficiency [10]. Figure 2 shows the three inventors measuring the power output of one of their first devices.

Figure 2. (From left) Gerald Pearson, Daryl Chapin and Calvin Fuller, the inventors of the silicon solar cell, measuring electrical energy produced by one of their first devices under a lamp. From the Lucent Technologies web site: www.lucent.com.

Today, solar cells and modules can be divided into two main categories: wafertype and thin film. Wafer-type cells are made from silicon wafers cut from a rod or ingot, or from silicon ribbons. Thin film cells are deposited directly onto a substrate, usually glass, stainless steel, or plastic. For flat-plate applications, the individual cells are connected in series to form a module. Solar cells for concentrator systems are mounted in a one-dimensional or two-dimensional optical concentrator. Typically, conversion efficiencies for commercial photovoltaic modules range from 8–15% depending on type of material and fabrication technology.

Photovoltaics is used in a wide variety of applications, from consumer products and small standalone units for rural use such as solar home systems and solar lanterns, to grid-connected rooftop systems and large power stations. Typical system size varies from 50 W to 1 kW for standalone systems with battery storage, from 500 W to 5 kW for rooftop grid connected systems, and from 10 kW to several MW for grid connected ground-based systems and larger building integrated systems. Within these market segments, rural electrification for sustainable development and building integrated systems are expected to grow rapidly because of concentrated marketing efforts and financial incentives [4].

1.3 The photovoltaic system

A photovoltaic system consists of solar cells and ancillary components such as power conditioning equipment and support structures. Solar cells, which are semiconductor diodes, convert sunlight directly to electricity through the photovoltaic effect. The cells are normally strung together in various physical and electrical configurations to form a module. When several of these modules are mounted in a cluster and connected in series and/or in parallel to provide the required voltage and current levels, the collection of the closely fitting modules is often referred to as an array. The resulting electrical power is processed through an appropriate power conditioning unit to meet the requirements for various applications. If

energy storage is desired, it may be included as part of the system, or the system may be tied to an existing grid. In many applications, storage may not be required or used. Figure 3 shows schematically a typical photovoltaic system.

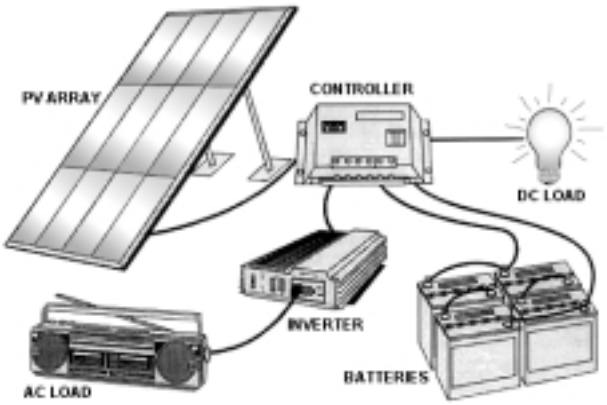

Figure 3. Schematic picture of a photovoltaic system From the Solar Wind Works web site: www.solarwindworks.com.

The solar array is usually mounted on a metal structure and tilted to face the sun. If the system is of stand-alone type, a charge controller maintains the batteries at the proper charge rate, and protects them from overcharging. The battery bank contains one or more deep cycle batteries, connected in series and/or in parallel depending on the required voltage and current capacity needed. The appliances, for example lights, radios, water pumps or microwave repeaters, are either AC or DC driven. When using AC devices, an inverter is required. The inverter converts the DC power from the solar array and batteries, into AC power. The so-called Balance of System components provide the interconnections and standard safety features required for any electrical power system. These include array combiner box, properly sized cabling, fuses, switches, circuit breakers and meters.

1.4 Photovoltaic applications

Log on to the Internet, make long distance calls, turn on your cellular, watch TV, get the latest weather report, and you have most likely relied on photovoltaics. That is because solar cells power every telecommunication satellite and a good deal of land based telecommunication networks that forms the basis for the information highway. Solar cells also ensure the safe passage of ships and trains, by powering navigation and railroad warning devices. In fact, the use of solar cells already benefits hundreds of millions of people throughout the world.

As one of the first pilot applications, solar cells were used to power a telephone relay system near Americus, Georgia, USA in the mid 1950s. Technically, the system was a success, but an economic analysis revealed that the sun-powered unit was not competitive with conventional energy sources. The problem lay in the high cost of the pure-grade silicon required for the manufacture of efficient cells, and in the expensive, labor-intensive method of cell production. But just as it seemed certain that solar cells would be discarded as a case of poor economics, the

American space program created fresh interest in the technology. The space program needed a long-term reliable power source for its satellites, and since there is continuous sunlight in space, solar electricity require no storage and is therefore the lightest per watt source of power. The space program created and sustained a solar cell industry, and solar cells have powered almost every satellite since the late 1950s. Most of today's production of solar cells goes into two big market sectors; grid connected installations in industrial countries, and off-grid systems in developing countries.

1.4.1 Building integration

Building integrated photovoltaics (BIPV) is the integration of photovoltaics into buildings by replacing conventional building materials. For example, roofing materials might be replaced with architecturally equivalent solar modules that serve the dual function of building skin and power generator. As the building constructors are saving the costs of conventional materials it becomes more economical to buy and use photovoltaics. BIPV systems can either be connected to the available utility grid or be designed as stand-alone, off-grid systems. Many industrialized countries have national programs for building integration of photovoltaics. In Europe, Germany has been the most aggressive promoter, with a heavily subsidized program supporting the installation of 100 000 rooftop photovoltaic systems (www.100000daecher.de). In the USA was recently announced a solar roofs program that aims to install solar panels on one million roofs in America by 2010 (www.eren.doe.gov/millionroofs/). In Asia, Japan is the driving force, currently with a program that aims at building 70 000 solar homes and installing 4600 MW of photovoltaics by 2010 [11]. One of the benefits of grid-connected BIPV systems is that on-site production of power is typically greatest at or near the time of a building's peak loads. This provides energy cost savings through peak shaving and demand-side-management capabilities. Because photovoltaic collection areas can be extensive, they may have a significant impact on building design. Therefore, it is important to involve architects, constructors, and the local power utility from the earliest stage of a BIPV project.

1.4.2 Developing countries

One of the most important aspects of photovoltaics is the independence of the grid. Just as the Bell researchers in the 1950s foresaw that photovoltaics would be used to power applications in remote areas, rural electrification is still where solar electricity can have the largest impact on peoples standard of living. Solar cells can bring basic services, such as abundant clean water, electric lighting, and telephone service to the more than two billion people living in remote areas without access to the grid. Figure 4 shows an example of solar home systems, in this case providing electricity for fluorescent lighting in the village of Cacimbas in Ceara, Brazil.

Figure 4. Photovoltaics contributing to the sustainability of global civilization by providing clean, abundant energy. 50-watt solar home systems provide electricity for fluorescent lighting in the village Cacimbas in Ceara, Brazil. Courtesy US National Renewable Energy Laboratories.

Solar power in developing countries is primarily used for household lighting and radio and television. By extending the hours of available light it creates extra time for productive activities such as sewing, basket-making and handicrafts, and lets children continue studying after dark. Here, photovoltaics is a uniquely attractive source of electricity. The technology is already cost-competitive with traditional alternatives such as kerosene lamps and small diesel generators. Compared to energy from fossil fuels, solar energy systems are flexible, low maintenance and environmentally benign, but they have their limitations. The largest problem is that farmers will generally not be able to afford solar systems. Furthermore, batteries to store solar electricity can be costly and problematic. A backup system is required for nighttime and days with little sunlight, and disposal of the batteries poses an environmental threat [12].

While solar home systems are beginning to have an impact, the potential of solar energy is still relatively un-tapped within increasing agricultural productivity and rural development in general. With a supportive financial and institutional environment, small- to medium sized solar powered electricity generation plants feeding into local village community grids could significantly improve larger scale activities such as health care, education, water supply, communication, and tourism. To fully exploit the potential of solar energy will require several institutional changes in the energy sector [12]. Rural and agricultural development banks must make solar energy systems eligible for loans. The systems must be made more attractive to private investors. Above all, the energy, agriculture, education and health sectors must work together to promote solar technology, improve maintenance and servicing infrastructure, and create sustainable markets for the creation, use, and funding of solar energy systems.

2 Photovoltaic technologies

After the silicon photovoltaic cell was announced in 1954, it would take another 20 years until the interest for using solar cells for large-scale power production was awakened. A direct cause of the increasing interest was the first oil crisis in 1973. Up until then, solar cells were considered as high-cost devices for space applications only. During the past three decades, extensive research and development efforts have been devoted to finding new materials and fabrication processes with a higher potential of cost reduction than that of the crystalline silicon technology. But still today, the demand for solar cells is covered mainly by thick film crystalline silicon. In 1997, crystalline silicon accounted for nearly 90% of the module production [3].

The silicon technology has proven excellent stability and reliability, with modules operating under outdoor conditions over several decades, showing none or only minor deterioration in performance. At present, the barrier for adopting solar cells on a global scale is directly related to the high cost of electricity generated by solar cells. The high costs associated with the thick film crystalline silicon cells are mainly due to the high energy demand for purification of SiO_2, i.e. sand to silicon, and to low material yield during the fabrication process. The photovoltaic industry relies mainly on reject silicon from the microelectronics industry feedstock. With the growth of the photovoltaic industry, this source of feedstock is becoming insufficient. The supply of silicon will remain a serious bottleneck until high capacity production plants for solar-grade silicon are set up in order to supply a cheaper and less pure form of silicon than what is currently used in the microelectronics industry.

One of the most promising ways to achieve economical competitiveness of photovoltaics is to turn to thin film technologies. Thin film approaches are usually thought of as those utilizing active semiconductor material of approximately 10 μm or less in thickness. Thin film solar cells are composed of several thin films deposited on low-cost backing materials such as ordinary window glass, or alternatively, thin, flexible substrates such as metal or polymer foils allowing for roll-to-roll deposition processes with potential for additional cost savings. By using direct bandgap materials that have high absorption coefficients, the constraints on minority carrier lifetime and absorber thickness are less rigorous than for thick film crystalline silicon cells. Therefore, the thickness of a thin film device can be only a fraction of that of thick film crystalline silicon cells. Another specific advantage of the thin film technology is the possibility to grow large-area modules at once.

An alternative approach to reduce the cost of photovoltaic energy is using concentrator technologies to partly replace relatively expensive semiconductor material with module parts made of cheaper materials such as plastics for lenses or aluminum for reflectors. However, in this case factors such as ease of manufacture and scale-up, availability of direct sunlight, and cost of tracking the sun become increasingly important. There are two common approaches to concentrators – one uses line focus lenses or reflectors with concentration ratios in the order of 2–20, and the other uses point focus lenses with concentration ratios of up to 1000.

2.1 Crystalline silicon solar cells

Silicon has been and continues to be the foundation for the photovoltaics industry. The material is abundant, comprising about 20% of the earth's crust. Because of its

importance to the electronics industry, more is known about the properties of silicon than of any other semiconductor material. Silicon solar cells are made using either single-crystal wafers, multi-crystalline wafers or thin films. Single-crystal wafers are sliced (approximately 200–300 um thick), from a large single-crystal ingot, which has been grown at around 1400 °C in a very energy-intensive process. The silicon must be of a very high purity and have a near perfect crystal structure. The best single-crystalline silicon cells produced in research laboratories are at the 22–24% level [13]. However, such record cells are based on sophisticated designs and fabrication processes that are less suitable for large-scale commercial utilization. In going from small-size, expensive laboratory cells to large-area, low-cost commercial modules, various additional losses as well as compromises between performance and cost will result in modules with efficiencies in the 15–18% range [13].

Multi-crystalline wafers are commonly made by a casting process in which molten silicon is poured into a mould and allowed to set, after which the ingot is sliced into wafers. As multi-crystalline wafers are made by casting they are significantly cheaper to produce, but not as efficient as single-crystalline cells. The lower efficiency is due to imperfections in the crystal structure resulting from the casting process. For both the single- and multi-crystalline technologies, almost half of the silicon is lost as kerf in the slicing process. Efficiencies of high-end laboratory multi-crystalline silicon cells are in the 17–20% range, while commercial modules are at the 14–15% level [13].

The present cost of crystalline silicon modules is approximately 4 USD per W_p. In order to reduce the cost, there are several new approaches emerging for fabrication of thick film silicon wafers, in particular for multi-crystalline silicon cells, but the inherent fabrication obstacles of both the single- and multi-crystalline technologies are hard to circumvent. Even with a considerable increase in production volume, crystalline silicon technologies are not likely to meet the substantial cost reductions that are necessary for large-scale production of solar cells.

2.2 The thin film approach

The first true thin-film solar cells, Cu_2S/CdS, were originally developed for space applications with the promise of better power-to-weight ratio than crystalline silicon devices. High efficiencies were quickly achieved, and several companies were established to commercialize this technology [14]. However, due to inherent reliability problems [15] most research work on Cu_2S/CdS solar cells was terminated by the mid 1980s. To date, there are three major thin film technologies candidating for large-scale production. These are based on amorphous silicon (a-Si) or the multi-crystalline compounds cadmium telluride (CdTe) or copper indium gallium diselenide (Cu(In,Ga)Se_2 or CIGS). a-Si modules have been on the market for many years primarily in consumer-type applications such as pocket calculators, and are since a few years available also as full-size modules for power generation. CdTe is in the startup phase for a first pilot production line [16], while the CIGS technology has just recently been commercialized [17]. There are also hybrid approaches such as combined crystalline silicon-amorphous silicon cells. In addition, work is being done to develop thin film crystalline silicon solar cells. The following sections give an overview of the three thin film technologies that are closest to the commercial reality.

2.2.1 Amorphous silicon (a-Si)

Hydrogenated amorphous silicon was introduced as a material with a potential for semiconductor devices in the mid 1970s [18] and is the first thin-film solar cell material that has reached the stage of large-scale production. Amorphous silicon has a higher optical absorption coefficient than crystalline silicon and, thus, can be efficient at much less thickness. In order to reduce recombination losses, amorphous silicon solar cells are based on a *p*-*i*-*n* structure, consisting of a thin *p*-type doped layer, a central intrinsic *i*-type layer as the photon absorbing layer, and a thin *n*-type doped layer. The electrical transport in the *i*-type layer is assisted by an electric field.

Amorphous silicon solar cells are commonly deposited on glass coated with a transparent front contact of either SnO_2 or ZnO. The most widely used deposition technique is plasma enhanced chemical vapor deposition (PECVD). At present, industrial fabrication processes for large-area amorphous silicon are limited by rather low deposition rates, and the devices suffer from low efficiencies. One of the main reasons for the limited efficiencies is the Staebler-Wronski effect of light-induced degradation [19], due to which the efficiency decreases after extensive illumination. Typically for commercial amorphous silicon modules, an initial efficiency drop of about 25% followed by stabilization and mild oscillation around the stabilization point can be expected. Amorphous silicon cells in a tandem- or triple-junction structure has the potential for improved efficiencies by better utilizing the solar spectrum. Typically, efficiencies of stabilized triple-junction laboratory cells reach the 13% level, while commercial triple-junction modules have stabilized efficiencies in the 4–8% range [20]. The price of amorphous silicon solar modules is still today, for a given stabilized power output, only marginally lower than that of crystalline silicon modules.

2.2.2 Cadmium telluride (CdTe)

Thin films of cadmium telluride receive much attention as absorber materials for efficient, low-cost solar cells. CdTe devices are commonly based on a CdS/CdTe hetero-junction, and laboratory cell efficiencies as high as 16% and large area modules at the 9% level have been reported [21]. Their advantages include direct bandgap with nearly optimum value for photovoltaic applications, and good match of the electron affinity to the cadmium sulfide window.

Based on predictions of optimum bandgap for solar conditions, CdTe was suggested as a photovoltaic compound in 1959 [22]. The first efficient devices based on the CdS/CdTe structure was accomplished in 1972 [23], and soon devices with conversion efficiencies exceeding 10% were fabricated by screen-printing. The first commercial product was released in 1982, but withdrawn again because of stability problems related to degradation of the electrical contact to the CdTe film [24].

CdTe films have been deposited by a variety of methods, including electro-deposition, screen-printing, and high-rate evaporation, but the best performing CdTe-based devices are fabricated using closed-space sublimation [21]. The raw materials, cadmium and tellurium, are relatively inexpensive and available in reasonable quantities. Cadmium is classified as an environmentally hazardous material, but the compound CdTe itself is reported to be very stable [25]. Advances in process development at the laboratory scale have been gradually transferred to large-scale deposition and module fabrication. The most important players within

commercialization of the CdTe technology are Matsushita in Japan, Antec in Germany, and First Solar and BP Solar in the USA [26].

2.2.3 Copper indium gallium diselenide (CIGS)

Copper indium diselenide (CIS) is a *p*-type multi-crystalline semiconductor with high optical absorption coefficient. For thin film solar cell applications, this compound is used in a heterojunction structure, commonly with a very thin *n*-type cadmium sulfide layer. The optimal bandgap for a single-junction solar cell with respect to the solar spectrum is around 1.4 eV [27]. Pure $CuInSe_2$ has a bandgap of 1.04 eV. To increase the bandgap, indium can be partially replaced by gallium, thus obtaining copper indium gallium diselenide (CIGS). An indium to gallium ratio of 20–40% will result in a bandgap of approximately 1.1–1.2 eV which has been shown empirically to give the best cell results. The bandgap of pure $CuGaSe_2$ (CGS) is 1.67 eV. A further degree of freedom is achieved by the partial substitution of Se_2 for S_2 (CIGSS). The direct bandgap and the high absorption coefficient of CIGS relaxes the requirements on minority carrier lifetime and facilitates thinner absorber layers since the photo-excited carriers are generated close to the depletion region [28]. This makes CIGS a suitable compound for thin film solar cells.

CIGS thin film solar cells have been fabricated by several research groups at over 15% efficiency, and the efficiency record obtained for a small laboratory cell is as high as 18.8% [29]. Laboratory mini-modules have reached 16.6% efficiency [30]. In terms of stability, CIGS solar cells do not have the problem of light-induced degradation. On the contrary, they tend to exhibit a slight increase in open circuit voltage and in efficiency during the first hours of operation. CIGS devices have shown promising results in outdoor long-term performance tests [31], but at the same time they are more sensitive than for example crystalline silicon solar cells to hot and humid environments [32].

$Cu(In,Ga)Se_2$ is considered to be one of the most promising materials for large-scale fabrication of low-cost high-efficiency thin film solar cells, and as device results are approaching two of the important milestones on the route to commercialization – the 15% efficient module and the 20% cell – several research institutes have announced their plans for CIGS production lines. The first, and so far the only, commercial CIGS module was released in 1998 by Siemens Solar Industries [17], but the US-based production is still on a limited scale. It is expected that CIGS modules in mass production will be substantially cheaper than wafer-based crystalline silicon modules. Module production costs of less than 1 USD per watt peak is commonly forecasted [11]. Much of the current research activities in the CIGS field are directed towards manufacturability issues such as technology scale up, module design, packaging, and long-term stability. Other hot research topics are the possibilities to reduce the amount of indium used, and to remove or to find a less hazardous replacement of the thin cadmium sulfide layer.

2.3 Concentrator systems

Concentrating sunlight onto high efficiency solar cells has the potential to yield lower electricity costs than conventional photovoltaic power systems. The challenges for solar concentrator systems are to utilize cheap mirrors or lenses which can accurately concentrate the sun onto an area of photovoltaic modules, to

reliably and accurately track the sun, and to adequately cool the solar cells to maintain a high power output.

The idea with concentrating photovoltaic systems is to partly substitute the relatively expensive photovoltaic absorbers with cheap light concentrating devices. Concentrators can be of various types. For low concentration ratios (up to 20–30) different types of reflectors or mirrors are most common, while lenses made from glass or plastic are normally used at higher concentration ratios. The lenses can concentrate the sunlight as much as 1 000 times. Since the reflector or lens material is often far less expensive than the semiconductor absorber, this may seem a cost-effective way of boosting module output. Furthermore, modules operating in concentrated light exhibit higher efficiencies, which additionally lower power costs. However, concentrator systems are inherently more complicated than conventional flat-plate photovoltaic systems. Since concentrator cells are not able to use the diffuse component of the sunlight, most high-concentrating systems must track the sun to remain perpendicular to the incoming direct beam radiation. Concentrators therefore need to be mounted on tracking devices that follow both the sun's daily and its seasonal movement across the sky. Trackers add both mechanical complexity and operation and maintenance requirements to the system.

Efficiency of photovoltaic cells is temperature dependent. For most type of cells, the efficiency decreases with increasing temperature. Since a typical solar cell operate at 10–15% conversion efficiency, only a small fraction of the incoming solar irradiation is converted to electricity. A major fraction of the remaining irradiation is dissipated as heat in the absorber material. Typically, the operating temperature for conventional flat-plate photovoltaic modules will be 20–25 °C above the ambient temperature, lowering the efficiency about 10% relative. For concentrator systems, this is much more of a problem. Even at concentration ratios of only 4, a photovoltaic module will easily reach a temperature of 80–100 °C, resulting in drastic performance loss, and, in a worst case, permanent damage of the module. Therefore, the temperature of modules in concentrator systems must be controlled either by passive or active cooling. The energy extracted by active cooling, for example by circulating water, may be used in various ways, for example to heat tap water. Of course, this will further increase the complexity of the system.

Despite the additional complexity, many engineering experts believe that electricity produced from concentrator photovoltaic systems will be more economical per watt than conventional flat-plate systems that operate under non-concentrated sunlight, once the systems are produced on a large scale [33]. The reduction in expensive semiconductor material requirements, the high efficiency of concentrators, and the additional energy extracted as heat, is expected to compensate for the additional costs of tracking and cooling.

3 Fabrication and characterization of CIGS-based devices

$CuInSe_2$ was first synthesized by Hahn and co-workers in 1953 [34], but not until 1973 it was proposed as a photovoltaic material by Wagner and co-workers, who reported on a single-crystal based cell with an efficiency of 12% [35]. Large progress in the development of multi-crystalline CIGS solar cells was made by Boeing Corporation during the early 1980s, when an efficiency higher than 10% was achieved with a three-source co-evaporation process [36]. By using a different process, based on selenization of stacked metal layers, Arco Solar achieved cell efficiencies as high as 14.1% in 1987 [37]. Arco had the intention of commercializing their technology, but due to poor reproducibility and low production yield, the envisaged pilot production was considerably delayed. Not until 1998, long after Arco Solar had become Siemens Solar Industries, the first commercial products was introduced to the market [17]. Initially, Siemens released a series of 5- and 10-watt modules produced at the pilot plant in California, USA. To date, the Siemens plant is fabricating up to 40-watt modules, and the production capacity is expected to reach 10 MW_p before the year 2005 [38]. Another important player in this field is Würth Solar, GmbH & Co. KG, who is operating a 1.2 MW_p pilot production facility in Marbach, Germany, aiming at scaling up to 10 MW_p [39]. Global Solar Energy Inc. have a slightly different approach to take market shares by aiming at niche applications where lightweight, flexible solar cells are valued [26]. Currently, Global Solar's prototypes are being evaluated in military field exercises under the supervision of the US Department of Defense. In addition to the organizations mentioned above, there are a number of companies which are at early stages of commercialization. These include Siemens Solar GmbH in Germany [38], Showa Shell Sekiyu K.K. in Japan [40], and the three American companies Energy Photovoltaics Inc., International Solar Electric Technology Inc., and Unisun [26].

3.1 State-of-the-art

As a result of the extensive research efforts during the past decade, a CIGS-based mini-module with an efficiency of 14.7% [41] and a gridded mini-module with an efficiency as high as 16.6% [30] have recently been reported. In addition, an 18.8% efficient small-area cell has been confirmed [29]. Figure 5 shows the history of CIGS efficiency records as found in the *Solar Cell Efficiency Tables*, periodically published since 1993 in *Progress in Photovoltaics*. Only cells larger than 1 cm^2, mini-modules smaller than 100 cm^2, and large-area modules above 3000 cm^2 are reported.

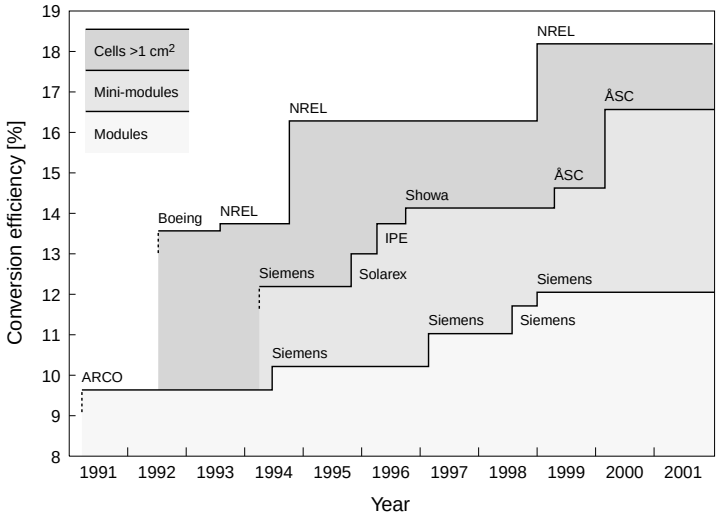

Figure 5. Evolution of CIGS record efficiencies in the past decade. All data are taken from the Solar Cell Efficiency Tables published in Progress in Photovoltaics.

In Figure 5 it can be seen that the evolution of the mini-modules is basically parallel to that of the record cells, the progress in the large modules possibly being slightly slower. Small cells can be used to achieve proof-of-concept record efficiencies, but they can also be used to show control and quality of economically viable baseline processes. However, small cells have no real product applications, and an increasing number of groups are working with, and producing, mini-modules. This serves to develop technologies, as well as to learn optimization schemes for full size module production. Taking the step from the mini-module scale to full-size modules is only an increase in substrate size, where the most critical issues are those of substrate temperature as well as compositional and thickness uniformity. For both cells and mini-modules, record efforts deviate from baseline efforts by a relaxation of the scalability, cost, yield, and throughput concerns.

CIGS devices are typically fabricated in a substrate configuration by sequentially depositing metal and semiconductor layers on a suitable base substrate (see Figure 6). The substrate is an important part of the device – not only does the quality of the substrate influence the properties of the device, but also the reproducibility of the fabrication process [42]. Ceramics as well as metal and polymer foils can be used as substrates, but most common is soda-lime glass.

The first layer deposited on the substrate is the molybdenum back contact, which serves as a conductive path for the photo-generated current and provides a good contact to the *p*-type CIGS absorber. Molybdenum has proven to have a number of important properties, such as tolerance to the relatively high process temperatures during CIGS growth, resistance to alloying with copper, indium, and gallium [43], and good contact properties. DC magnetron sputtering is the dominant deposition technique for the molybdenum back contact. It is a well-established industrial process with high throughput capacity [44].

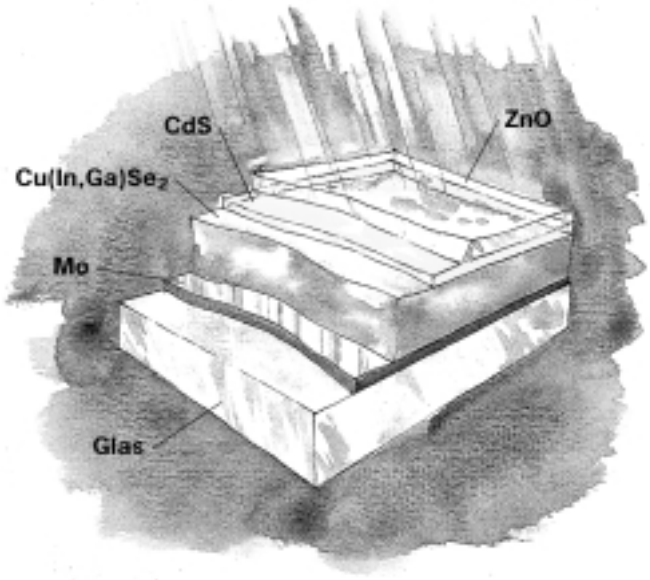

Figure 6. The structure of Cu(In,Ga)Se_2-based thin film solar cells in substrate configuration. Courtesy Jan Sterner, Ångström Solar Center.

For growing the Cu(In,Ga)Se_2 film, there are mainly two different approaches. In the first method called selenization, precursor layers of indium, gallium, and copper are first sputtered onto a substrate and thereafter selenized by annealing in H_2Se or elemental selenium vapor [40]. With the other method the elements are co-evaporated onto a heated substrate. This generally yields better laboratory efficiencies, but has less good prospects for up-scaling [26]. Most CIGS-based solar cells use a window structure consisting of chemical bath deposited cadmium sulfide, and a bi-layer of high and low resistive sputtered ZnO.

3.2 Baseline processing

At the Ångström Solar Center a *baseline* device recipe has been implemented, in which all steps in the fabrication, from substrate purchasing to device measurements, are defined for maximal simplicity and statistical significance [41]. The baseline gives a well-defined reference level for the experimental work as well as serving as a prototype of a pilot production. The criteria for selection of the process steps in the baseline are a combination of device superiority, process simplicity, potential cost, and statistical significance of the result.

Figure 7 shows a transmission electron micrograph of the cross section of a baseline CIGS device, and the fabrication process for each of the layers in the device are discussed in the following sections.

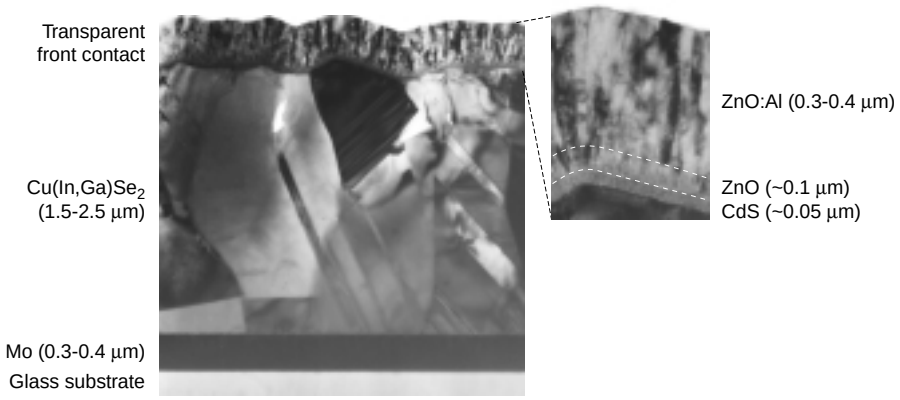

Figure 7. Transmission electron micrograph of the cross section of a baseline CIGS device.

3.2.1 Glass substrate

In the baseline, devices are fabricated on soda-lime glass substrates. These are either 2 mm thick standard float glass or 1 mm thick low-iron glass. Soda-lime glass is preferred because of its low cost, well matched thermal expansion coefficient to the absorber layer, high surface quality, and its chemical composition. The substrates are cut and ultrasonically cleaned using soap and water heated to 60 °C, followed by thorough rinsing and spin drying under blowing nitrogen.

3.2.2 Molybdenum back contact

The nucleation and growth of $Cu(In,Ga)Se_2$ grains are directly influenced by the thermal, morphological and chemical properties of the molybdenum back contact. It has been found that the use of soda-lime glass substrates results in high concentrations of sodium both in the molybdenum and in the CIGS [45]. During CIGS deposition, sodium diffuses out of the glass, through the molybdenum, and affects the $Cu(In,Ga)Se_2$ formation in a favorable way, resulting in large grains and high film density [46]. A considerable effort has been put into understanding the properties of the molybdenum back contact and to establish a good baseline recipe [44] for this process step. In the current baseline, the molybdenum back contact is grown at a thickness of 250–400 nm by a single pass in an in-line DC magnetron sputtering system.

3.2.3 $Cu(In,Ga)Se_2$ absorber

The $Cu(In,Ga)Se_2$ absorber is formed by co-evaporation from open boat sources using mass spectrometry control. Three 5×5 cm^2 substrates are loaded in each run, and the substrates are mounted onto a graphite plate and heated from the backside by quartz halogen lamps. The pressure in the chamber is typically 10^{-6} mbar, and the substrate temperature is constant and set at 510 °C during the 60 minutes of CIGS growth. The thickness of the absorber is between 1.5 and 2 μm, with a typical gallium to indium plus gallium ratio at the 25% level. There is no intentional use of any compositional gallium grading through the depth of the CIGS layer, nor is there any additional sodium precursor. The fact that the evaporation sources are physically separated will result in compositional gradients laterally across the samples. In spite of this, devices with comparable performance can be

prepared from all samples in a deposition run, which indicates a considerable compositional tolerance. In order to avoid oxidation of the absorber, which is known to have a negative effect on device performance [47], the thin cadmium sulfide buffer layer is deposited shortly after absorber growth. With this film as a protective coating, samples have been stored for several months in room temperature prior to completing of devices without noticeable impact on device performance.

3.2.4 Cadmium sulfide buffer

The thin cadmium sulfide buffer layer is prepared by chemical bath deposition. The film is formed by immersing the substrate in a cold alkaline aqueous solution containing 1M ammonia, 0.3M thiourea and 0.01M cadmium acetate. The reaction vessel is placed in a water bath at 60 °C. The deposition rate is determined by the temperature, pH and the relative concentrations of the chemical reactants [48]. A deposition time of around seven minutes is required to reach the desired film thickness of about 50 nm.

3.2.5 ZnO/ZnO:Al Window

Devices are completed using a bi-layer of high- and low-resistive ZnO. Both the 50–100 nm thick high resistive ZnO and the 300–400 nm thick low resistive Al-doped layer are RF magnetron sputtered without intentional substrate heating. RF sputtering may be a process too slow for industrial application, but it produces high quality devices at the laboratory level. The sputtering system used in this work is equipped with two parallel ceramic circular 5-inch targets, one pure ZnO for the high-resistive layer, and one ZnO/Al_2O_3 (98/2 weight %) for the low-resistive layer. Pure argon, as well as $Ar\text{-}O_2$ mixes, are used as sputter gases. The substrates are placed under one target at a time, and substrate to target distance is fixed at about 10 cm. A base pressure of at least $7 \cdot 10^{-7}$ mbar is obtained before each sputter process.

The baseline recipe consists in pre-conditioning the targets in an $Ar\text{-}O_2$ mix, then pre-sputtering and sputtering the films in pure argon. Although this makes high quality devices, it is very wasteful in both time and target material. Therefore, an alternative process requiring neither pre-conditioning nor pre-sputtering has been investigated. In this process, which is called the “bleed”, very small quantities of oxygen are added to the argon during the deposition in order to sustain stable state conditions for continuous in-line deposition. The bleed process is further discussed in section 4.3.1.

3.2.6 Making cells and mini-modules

For making standard test cells, a 5×5 cm^2 device is cut into three 5×1.7 cm^2 stripes, each on which eight or maximum nine 0.5 cm^2 single cells are defined by mechanical scribing. The single cells are contacted by tapered finger grids in a 50/3000/50 nm thick Ni/Al/Ni sandwich. The nickel layers serve two purposes. The first layer improves the properties of the contact to the ZnO:Al, and the second layer protects the aluminum from long-term corrosion (see section 6.6.1). The grids are deposited by electron gun evaporation through a shadow mask and cover approximately 2.5% of the total cell area. Following the baseline recipe yields cell efficiencies in good control at the 14–15% level without the use of anti-reflective coatings.

When the baseline is used for mini-module production, the molybdenum back contact is patterned using photolithography while interconnect and isolation scribes are performed mechanically. Typically, the 20 cm^2 mini-modules have eight or nine cells and the total area efficiencies are in the 12–13% range. The efficiency deviation between cells and modules is further discussed in Chapter 4. A stripe of baseline cells and a mini-module is shown in Figure 8.

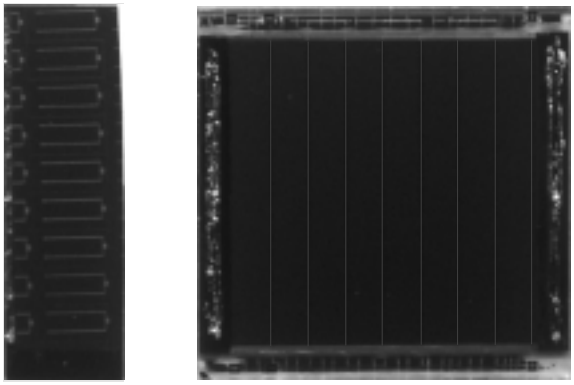

Figure 8. Photographs in 1:1 scale of a stripe of baseline cells and a mini-module.

3.3 Encapsulation

Since many manufacturers of crystalline silicon modules today give a 20 to 30 year warranty on their products, good long-term stability is an important requirement for any new photovoltaic technology entering the commercial scene. Photovoltaic modules in field conditions are subjected to a unique set of stresses that may alter their stability and, hence, their performance, both near term and in the long run. These stresses include ultraviolet radiation, elevated temperatures, daily as well as annual thermal cycles, atmospheric gases and pollutants, and, in concentrating systems, high-intensity irradiation. In addition, rain, hail, dust, wind, condensation and evaporation of water, thermal expansion mismatches, etc., may cause module failures [49]. A prerequisite for stability is that the materials that compose the solar cells are intrinsically stable. In addition, an encapsulation is needed to protect the devices from external stresses. Once the bulk properties of the module component materials are stable, the initiation of many degradative effects can be expected to occur at surfaces and interfaces. To prevent this, a proper encapsulation must be developed, where the collective action of all external stress factors are considered.

A good encapsulation fulfills the following criteria: it is cheap; it provides structural support; it gives a good optical coupling between the solar cell and the incident solar irradiation in the spectral region of interest; it provides physical isolation from exposure to hazardous or degrading environments; it provides electrical isolation of the solar cell circuit from both operational and safety viewpoints, as well as good thermal conductivity to avoid overheating; and it has an operational lifetime of 20–30 years [49].

Crystalline silicon modules are typically laminated between a cover glass and a backing substrate, using an encapsulant. To be economically and practically useful,

the encapsulant material has to meet the requirements of low cost, good processability, high optical transmission, high dielectric constant, low water absorptivity and permeability, high resistance to ultraviolet degradation and thermal oxidation, good adhesion, mechanical strength, and chemical inertness.

The encapsulant that has been used predominantly for the last decade by the photovoltaics industry is the ethylene vinyl acetate (EVA) copolymer, developed by US-based Jet Propulsion Laboratory and Springborn Laboratories in the early 1980s [50]. In a detailed survey of potential candidate encapsulants, EVA stood out as the most promising, mainly because of its relatively low cost. After many years of extensive research and development, EVA is today technically mature and fulfills most of the criteria listed above. A detailed review of the EVA-based encapsulation technology is given in [49].

In the present work, a prototype system for encapsulation of small-area laboratory CIGS devices has been developed. The setup, shown in Figure 9, consists of a temperature controlled hotplate and a two-chamber low-vacuum system. Firsts attempts to encapsulate mini-modules with various encapsulants such as EVA, thermoplastic, and silicones have yielded promising results. Accelerated lifetime tests where the various encapsulants are compared from a long-term stability point of view are discussed in section 6.7.

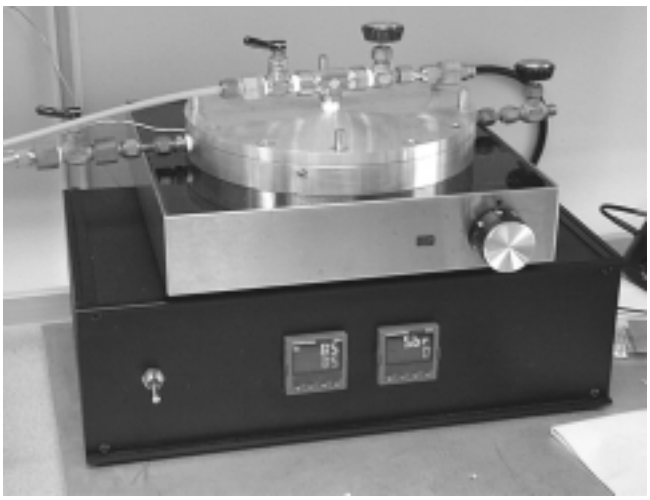

Figure 9. Prototype system for encapsulating small-area CIGS thin film solar cells.

3.4 Characterization techniques

In order to understand the possible relationships between the material properties and the final device performance it is necessary to investigate both the material characteristics and the electrical behavior of the CIGS solar cells. This section gives a description of the key characterization techniques applied in this work.

3.4.1 Current-voltage characteristics

Current-voltage characterization of small-area devices (up to 5×5 cm^2) is done in standard test conditions using a solar simulator based on a single 300-W ELH

tungsten-halogen light source with cold mirror, normalized to a light intensity of 100 mW/cm^2. Current and voltage are imposed by a computer controlled HP4142B monitor with a one-ampere HP41420A source monitor unit. The samples are placed on a temperature-controlled stage (25±1 °C) and contacted in a four-point probe configuration. In order to stabilize the devices prior to characterization, these are subject to post-growth treatment. In the current baseline the procedure for this is defined as 2+2 minute cycles of subsequent air annealing at 200 °C. The current-voltage measurement set-up with the solar simulator is shown in Figure 10.

Figure 10. Current-voltage characterization set-up.

As the tungsten-halogen light source ages, the spectrum is shifted towards longer wavelengths which, due to the cold mirror, will result in lower current values for baseline cells. This effect is compensated for by gradually lower the position of the lamp, thus bringing it closer to the device under test. The light intensity on the sample will still be 100 mW/cm^2 but at a slightly different spectrum. The expected service life of the lamp is 36 hours but to avoid to large shifts of the spectrum the lamp is regularly replaced after 30 hours.

As an external load is connected to the illuminated solar cell the current flow in the circuit can be seen as the result of two counteracting currents. The current-voltage characteristics can be described as

$$I = I_D - I_L = I_0(e^{\frac{qV}{AkT}} - 1) - I_L$$

where I is the total current, I_0 the saturation current, q the electrical charge, V the applied voltage, k Boltzmann's constant, A the diode ideality factor, and T the temperature. The photo-generated current I_L represents the light generation of carriers, while the diode or dark current I_D is given by the characteristics of the *p-n* diode [51]. The diode ideality factor depends on material characteristics such as doping and trap density, and typically has a value between 1 and 2 [51]. In theory, the light current-voltage curve is just the dark diode curve shifted by the light induced current. In reality, however, solar cells often behave differently in dark

and under illumination. Figure 11 shows the ideal current-voltage characteristics of a solar cell in dark and under illumination.

Under normal operation, the highest current value is obtained under short circuit conditions, i.e. at V=0, as seen in Figure 11. The short circuit current I_{sc} is given by

$$I_{sc} \equiv I(V=0) = I_L$$

while the open circuit voltage V_{oc} can be derived from the equation of the current-voltage characteristics as

$$V_{oc} = \frac{AkT}{q} \ln\left(\frac{I_L}{I_0} + 1\right)$$

The maximum power $P_{max} \equiv I_{max} \cdot V_{max}$ that can be produced is indicated by the area of the rectangle in Figure 11. From the maximum power point, the fill factor FF can be calculated. FF is a quantitative measure of the quality of the device through the squarness of the current-voltage curve, and is defined as

$$FF = \frac{V_{\max} I_{\max}}{V_{oc} J_{sc}}$$

The energy conversion efficiency η of a solar cell is defined as

$$\eta = \frac{V_{\max} I_{\max}}{P_{in}} = \frac{V_{oc} I_{sc} FF}{P_{in}}$$

where P_{in} is the total radiation incident on the solar cell.

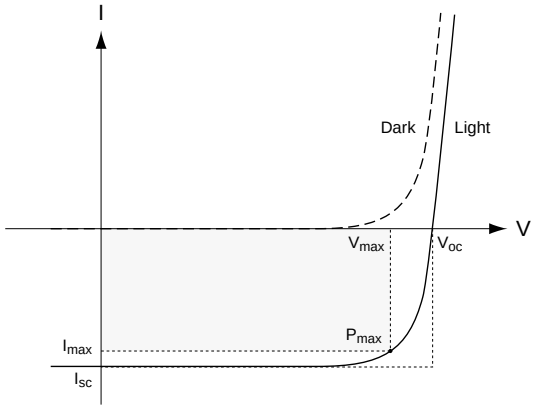

Figure 11. Current-voltage characteristics of a solar cell in dark (dotted line) and under illumination (solid line). Open circuit voltage (V_{oc}), short circuit current (I_{sc}) and maximum power point (P_{max}) are indicated.

The set-up shown in Figure 10 is not suitable for testing devices with areas larger than 5×5 cm^2. This is partly because the solar simulator produces relatively non-uniform illumination over larger areas. In Paper VI, commercial CIGS modules with areas of 30×30 cm^2, were tested in a large-area solar simulator at the

Division of Energy and Building Design, Lund Institute of Technology. This simulator uses seven Philips MSR 2.5 kW dimmable metal halide lamps, place in a honeycomb configuration with a maximum lateral width of 2.3 m. Compared to the solar spectrum, the spectrum of these lamps are slightly shifted towards shorter wavelengths. To obtain light as parallel as possible, each lamp is mounted in a combined parabolic and hemispherical reflector arrangement. In order to simulate the movement of the sun across the sky, the lamps are mounted on a movable frame, rotating around a horizontal axis through the center of the wall where the photovoltaic modules are mounted. The wall itself can rotate around a vertical axis. This arrangement is shown in Figure 12. Results from the measurements are further discussed in section 5.2.4. Additional technical details on the large-area solar simulator are given in [52].

Figure 12. Large-area solar simulator at the Division of Energy and Building Design, Lund Institute of Technology.

3.4.2 Temperature dependent current-voltage characteristics

Temperature dependent current-voltage {I-V(T)} measurements are done in both light and dark conditions. The I-V(T) set-up is based on an AET/Kel-Tran continuous flow cryostat with a Lakeshore 330 temperature controller and a Keithley 2400 source monitor unit. Measurements are done in vacuum at temperatures ranging from 100 to 380 K in steps of 20 K. A four-point probe configuration is used for contacting. The system is controlled by a PC with LabView software. The set-up is shown in Figure 13.

Figure 13. Set-up for temperature dependent current-voltage characterization.

3.4.3 Quantum efficiency

The quantum efficiency QE(λ) is the ratio of the number of carriers collected by the solar cell to the number of photons at a given wavelength of the incident light. It is often useful to look at the quantum efficiency of the light left after the reflected and transmitted light has been subtracted. The term internal quantum efficiency refers to the efficiency with which photons that are not reflected or transmitted out of the cell can generate current. By measuring the reflection and transmission of a device, the external quantum efficiency curve can be corrected to obtain the internal quantum efficiency curve.

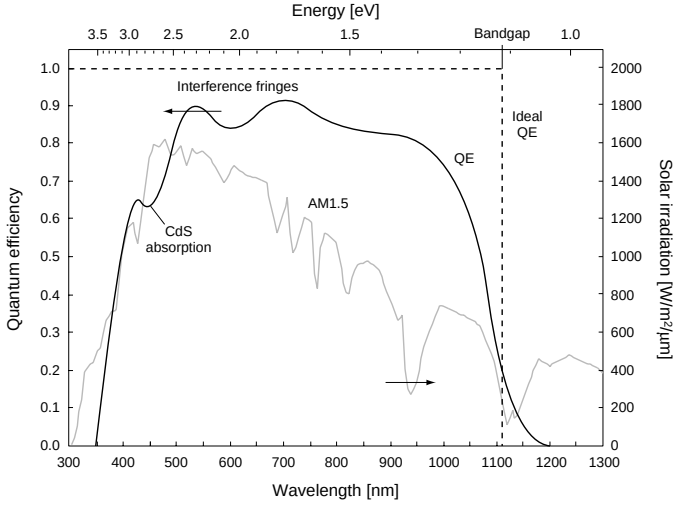

Figure 14. Typical wavelength resolved external quantum efficiency plot of a baseline CIGS cell.

Figure 14 shows a typical quantum efficiency plot of a baseline CIGS cell. This is the external quantum efficiency, i.e. it includes the effect of optical losses such as transmission and reflection. Ideally, the quantum efficiency is a square (dotted line), but in reality it is reduced due to recombination effects (solid line). The dip in the curve at around 450 nm is characteristic for CIGS solar cells and is caused by absorption in the thin CdS buffer layer. In addition, the curve often includes a number of interference fringes as indicated. A measure of the "true" short circuit current density of the device under test is obtained by integrating the quantum efficiency multiplied with the solar spectrum.

The quantum efficiency set-up used in the present work has a xenon light source, allowing measurements at wavelengths down to 360 nm. The light from the monochromator is chopped and transmitted to the sample by optic fibers for enhanced flexibility. The response signal from the device under test is fed through a lock-in amplifier, which facilitates light-bias measurements. System operation and data collection are controlled by a PC with LabView software.

3.4.4 Resistivity and figure of merit

The resistivity ρ of the films in baseline CIGS devices is routinely characterized by sheet resistance measurements using a four-point probe set-up. Figure 15 illustrates the probe configuration. A small current from a constant-current source is passed through the outer two probes and the voltage is measured between the inner two probes. For a thin film with thickness W much smaller than either a or d, the sheet resistance $R_{\square}$ is given by $R_{\square} = V/I \cdot CF$ [Ω/□], where CF is the correction factor shown by the curves in Figure 15. From this, the resistivity is calculated as $\rho = R_{\square} \cdot W$ [Ωcm].

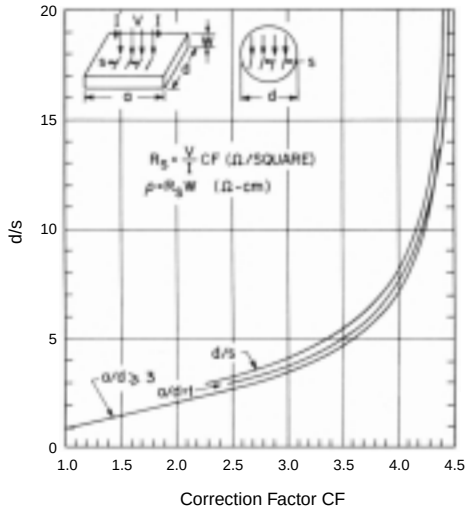

Figure 15. A four-point probe configuration with correction factor for measuring the sheet resistance of thin films. After [51].

For the ZnO:Al transparent front contact in particular, the sheet resistance is a useful measure of the status of deposition process. By introducing the figure of merit for the front contact process, the condition of the ceramic sputtering target

can easily be checked by measuring the sheet resistance of the deposited film. The figure of merit is expressed in terms of reduced current density due to optical losses in the front contact for a given front contact sheet resistance. Based on spectrally resolved transmission and reflection measurements, the current loss is calculated from the fraction of the available light within the wavelength range of the absorber quantum response, which is not transmitted through the front contact. This is schematically illustrated in Figure 16.

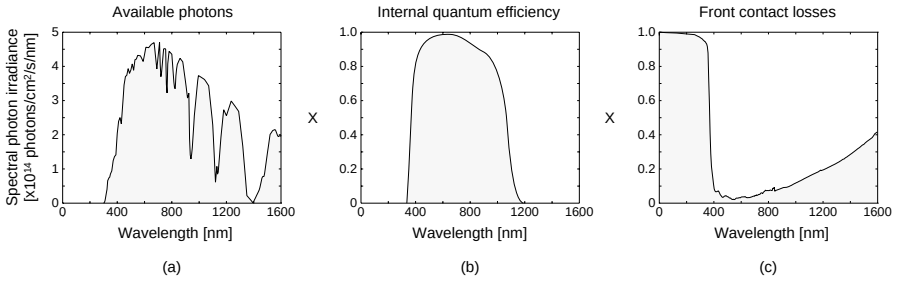

Figure 16. Current loss calculation for the ZnO:Al transparent front contact: The number of available photons in the solar spectrum (a) is integrated with the internal quantum response of the CIGS absorber (b), and with the measured optical losses (reflection plus absorption) in the front contact (c).

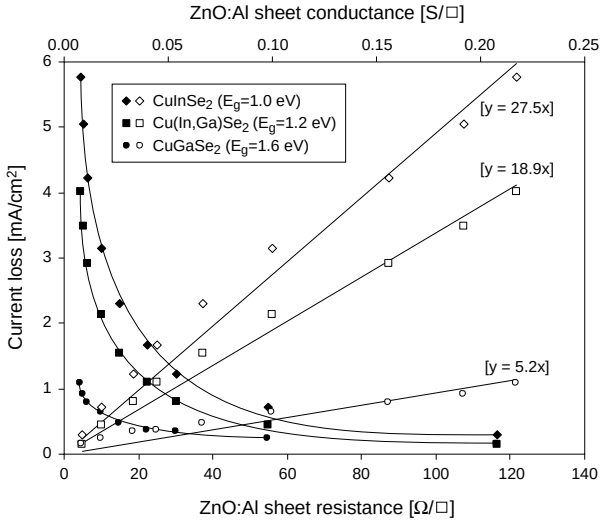

Figure 17. Experimentally obtained figures of merit for the baseline ZnO:Al transparent front contact, plotted for different absorbers. In each case, the figure of merit is given by the slope of the straight line.

The absorption of a material increases exponentially with the film thickness d according to $A \propto (1-e^{\alpha \cdot d})$, where α is the absorption coefficient. However, for small α, i.e. for low-absorbing materials, $(1-e^{\alpha \cdot d}) = 1 - (1-\alpha \cdot d) + \frac{1}{2}(1-\alpha \cdot d)^2 + \ldots \approx \alpha \cdot d$. Hence, for a given front contact deposition process, yielding low-absorbing films, the absorption and thus the current loss at a given absorber, should increase close

to linearly with the thickness of the front contact, while the sheet resistance is inverse proportional to the thickness. Plotting current loss against sheet conductance (the inverse of sheet resistance) should therefore yield a straight line, and the figure of merit is given by the slope of this line. The figure of merit is thus a unique number for a given absorber and a given front contact process. Best module efficiency, with respect to optical and ohmic losses, would be achieved by using the front contact process with the lowest figure of merit, i.e. the line with the smallest slope. This is demonstrated in Figure 17, where the current loss of the baseline ZnO:Al process is plotted for three different absorbers with different bandgaps, both against sheet resistance and sheet conductance. As further discussed in section 4.3, these kind of plots are useful when designing modules.

4 Design of CIGS-based modules

As discussed in Section 3.1 the development of cells and modules have proceeded more or less in parallel, although the efficiency levels of record modules always tend to be a significant step behind record cells as can be seen in Figure 5 above. From this, one might conclude that there is a large fundamental difference in performance between cells and modules. However, it is not relevant to compare best cell level to best module level. While modules are often fabricated with processes transposable to large-scale production, where homogeneity, yield, cost, parameter sensitivity and process simplicity are all critical for a successful result, the highest cell efficiencies reported are often achieved by using extreme conditions, far from fulfilling these requirements.

Nevertheless, there is often a noticeable difference in performance between cells and modules, also when fabricated with basically the same processes [53, 54]. This can partly be explained by non-uniform film deposition, which will affect the performance of small-area cells less than of larger-area modules. In addition, modules usually have a larger fraction of dead area, i.e. area that is not active in current generation. Furthermore, the quality of cell interconnects and the fact that optimization of the transparent front contact for modules is quite different from that of cells, contribute to this discrepancy. The problem of non-uniform film growth is related to up-scaling and manufacturability of the technology as such, and is not addresses in the present work. Here, the three major design issues considered are the interconnect structure, the transparent front contact, and the module geometry. These and other aspects on design of CIGS-based modules are discussed in Papers II, IV–VIII, and also briefly reviewed in the following.

4.1 Cell interconnects

As cells are integrated into modules, functional parts – interconnects – are added to the device structure. At the same time, various loss mechanisms are induced in the device. In particular, parasitic ohmic losses in the contacts, shunting of current between cells, and area losses due to scribing are significant effects. The efficiency gap between cells and modules can be reduced, to a large extent, by paying attention to these issues. The successful module design will always involve a trade-off of dead area versus ohmic losses, optical losses and leakage currents.

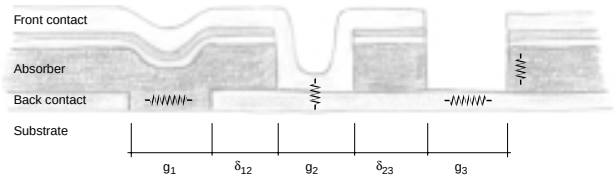

Figure 18. Standard interconnect design for CIGS modules based on the conventional Mo/Cu(In,Ga)Se_2/CdS/ZnO/ZnO:Al device structure.

The standard interconnect structure used for conventional CIGS modules is shown in Figure 18. This structure was originally developed for amorphous silicon modules [55], but has for a long time been used by many groups within the CIGS community as well [56, 57]. In the baseline process, the molybdenum back contact is patterned using photolithography while interconnect vias and isolation scribes

are performed mechanically. In the design of a module, it is important to consider not only the effects of resistive losses in the ZnO to Mo contact but also the shunt conductance through the CIGS in the back contact scribe. Furthermore, an optimized interconnect structure is a trade-off of dead area versus leakage currents and resistive losses.

For modeling of the standard interconnect structure in Paper IV, it was assumed that the total dead width $g_1 + \delta_{12} + g_2 + \delta_{23} + g_3$ is 400 μm, and that it is equally divided into the five sections shown in Figure 18. However, it is demonstrated in [56] and in Paper VII that the dead areas between the scribes can be eliminated with a sufficient control of the position of the scribes, and that the scribes can be made as thin as 25–50 μm width a good scribing technology, which would give a total interconnect width of 75–150 μm. Design of interconnects is further discussed in [58] and [59], as well as in Papers IV and VII, where, in the latter, modules based on different interconnect structures are realized experimentally and compared using power loss calculations.

4.2 Power loss analysis

A power loss analysis is a useful tool to understand in which parts of a module the losses occur, and to quantify these losses. In the present work, a spreadsheet model has been developed for calculating the power losses in modules. The model is used in Paper VII to justify the concept of gridded modules, and in Paper VIII to compare different module designs from a long-term stability point of view.

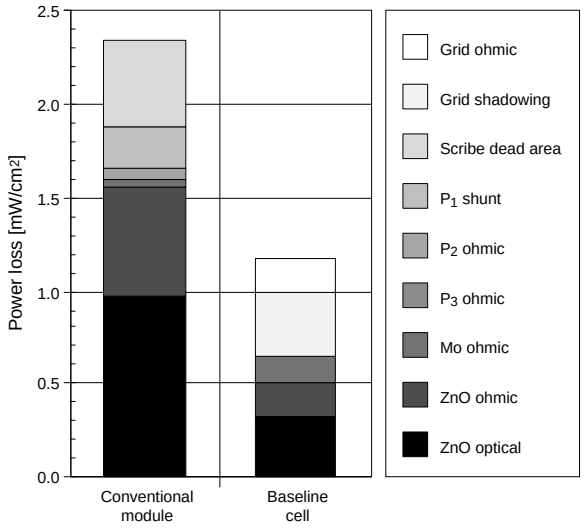

Figure 19. Power loss analysis, comparing a conventional module with a baseline cell. All losses are calculated relative to an ideal cell.

In Figure 19, the most significant losses for a conventional module are compared to those for a baseline cell. Here, the losses are calculated relative to an "ideal" reference cell based on a material quality of a 15% efficient cell exhibiting 30 mA/cm^2 at its maximum power point. This device is ideal in the sense that is has a totally transparent ZnO:Al front contact and no ohmic losses. From this

reference level, the additional power losses that are caused by optical absorption, parasitic resistances, shunting, dead area, and shadowing, are calculated for each device operating at its maximum power point. As can be seen, the baseline cell experiences losses with respect to the reference cell that are approximately 1.2 mW/cm^2, while the module losses are 2.3 mW/cm^2. The difference is mainly due to increased optical and ohmic losses in the front contact, which has to be thicker (i.e. more conductive and less transparent) than for cells, to achieve best module performance. As is discussed in the next section, optimizing the front contact is, to a large extent, a trade-off between its optical and electrical properties. Since the baseline cell has grids on top of the front contact, the current collection length is much smaller than for the module. Therefore, the cell can tolerate a more transparent, i.e. a less conductive, front contact, which results in lower optical losses.

The qualities of the power loss analysis are further described in Paper VIII, where the evolution of the losses during accelerated ageing is also discussed.

4.3 Optimizing the transparent front contact

One of the key issues in module design is optimizing the low-resistive aluminum doped zinc oxide transparent front contact. This layer has to be conductive enough to not cause too high ohmic losses and transparent enough to avoid severe optical losses. The ohmic losses depend on the conductance of the ZnO:Al as well as the module geometry, while the optical losses are determined by the optical properties of the front contact. Designing a module involves a trade-off between the electrical and the optical properties of the front contact.

There are two levels of front contact optimization. Firstly, the material used, in this case ZnO:Al, should be as transparent as possible for given electrical properties, i.e. its figure of merit (see section 3.4.4) should be optimized. This is achieved at the process level. Secondly, once the process is defined and fixed, a proper working point on the figure of merit curve is chosen. The working point, i.e. the current loss for a given conductance, is dependent on the segment width, or the lateral current collection length of the cells in the module.

4.3.1 Optimizing the process

In Paper II, a study on optimization of RF-sputtered ZnO:Al/ZnO films for baseline CIGS devices is presented. Here, two different processes are investigated; the baseline (see section 3.2.5) and what is called the bleed process. In the baseline process, the targets are preconditioned in an argon-oxygen mix, followed by pre-sputtering and sputtering the films in pure argon. Although this makes high quality devices, it is very wasteful in both time and target material. In the alternative bleed process, neither pre-conditioning nor pre-sputtering is needed. Instead, very small quantities of oxygen are added to the argon during the deposition so as to sustain stable state conditions for continuous in-line deposition.

In Paper II, the influence of power, pressure and flow on deposition rate, film conductance and transparency, at fixed pre-conditioning and pre-sputtering conditions, have been examined. The transparency is qualified using the current loss measurements and the trade-off between transparency and conductance is characterized by the figure of merit. Good reproducibility of the bleed process is proven for a gas mix with 0.5% oxygen. As can be seen in Figure 20, the figure of

merit obtained for the bleed process is similar to that of the baseline. Thus, the optical and electrical properties of the films are equal for the two processes.

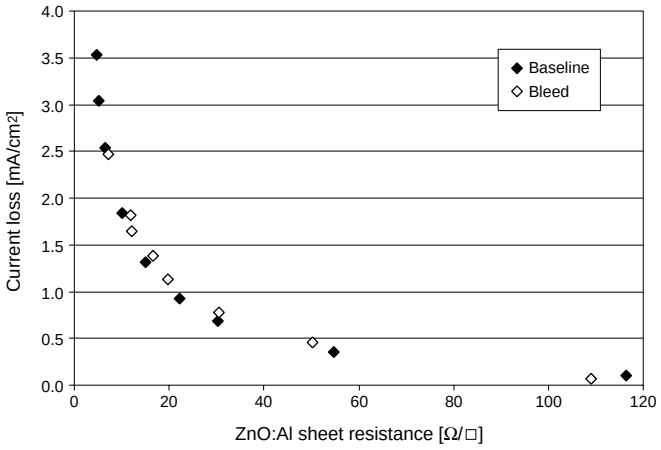

Figure 20. Figure of merit curves for two different front contact processes, calculated for the baseline absorber.

The basic open question is the influence of the oxygen on the interface of the growing device. It has been shown that having oxygen in the plasma can be harmful to the device in the conditions where the CdS is too thin [58]. However, from the experimental cell results obtained in Paper II it appears that both tested processes render equal device quality.

From a large-scale manufacturing point of view, processes that can run continuously are preferred over ones that require regular conditioning, and faster processes are preferred. Assuming equal device quality, the bleed process has the great advantage of being steady state and compatible with in-line deposition. It remains to be shown whether this process can be competitive with DC magnetron and DC reactive processes, which are generally considered to allow higher deposition rates than RF processes.

4.3.2 Choosing the working point

Once the deposition process is defined, the appropriate working point on the figure of merit plot must be selected. To illustrate the procedure, an example is given in Figure 21. This graph is calculated for a conventional module structure at one-sun illumination, using the software Module Design [59]. Here, the cell width (hence the maximum lateral current collection length) is optimized for maximum conversion efficiency as a function of the ZnO:Al front contact sheet resistance, taking into account the figure of merit for baseline absorbers that is shown in Figure 17. As input to the model is assumed baseline CIGS quality rendering 14.4% active area cells. Both the optimum cell width and the resulting module efficiency at each cell width are shown. In this case, a maximum efficiency of 12.2% is obtained for a module with 5 mm cell width using a ZnO:Al front contact at 10 Ω/□ sheet resistance. This is more than two absolute percent below the input cell efficiency, while it is argued in Papers VII and VIII that this difference can be less.

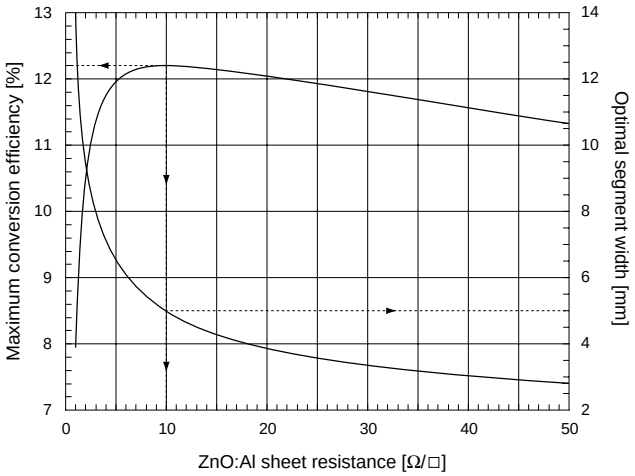

Figure 21. Calculated conversion efficiency of a conventional module at 1-sun illumination. Segment width is optimized for maximum performance at each value of the ZnO:Al front contact sheet resistance. The simulation is based on characteristics of a typical small area cell within the statistics of the baseline, having an active area efficiency of 14.4%.

In the production of modules the cell length is chosen and fixed, but the sheet resistance of the ZnO:Al transparent front contact may vary around its process target value. It is therefore important that the devices be tolerant to variations in the front contact process. Such a sensitivity study is presented in Figure 30 in section 5.3 for different module designs. For all designs presented, the performance will decrease for very conductive (i.e. thick) ZnO:Al due to the fact that the optical absorption becomes a dominant factor. Performance will also decrease for very resistive (i.e. thin) ZnO:Al as the resistive losses will dominate. Between these two extremes, each design will result in different values of the maximum module efficiency for different ZnO:Al conductivities, but more important is that they will have different tolerance to process variations.

Low-concentrated illumination can also be considered for CIGS devices as tests with various kinds of reflectors have shown promising results in order to reduce the cost of photovoltaic power. In this case, both the front contact process optimization as well as the choice of working point on the figure of merit curve will be different. In Papers IV and V, modules for 4-suns light intensity have been designed, fabricated, and tested. It is shown that the high current densities obtained at these light intensities will require that special attention is paid to avoiding resistive losses, particularly in the front contact, and a solution with metal grids assisting the front contact is investigated. This design is also shown to have advantages at normal 1-sun operation, where the greatest benefits are not enhanced performance but better window processing tolerance and throughput, as well as improved degrees of freedom of the module geometry. Design of gridded modules is further discussed in section 5.3.

4.4 The influence of gallium on module design

Thin film modules with high cell voltages can give increased efficiency through reduced resistive losses [58]. For CIGS solar cells, a higher voltage can be

achieved by increasing the gallium content. The influence of cell voltage on module design has been studied for CIGS modules in Paper VII, where cells at equal efficiency but fabricated from absorber materials with different bandgaps (i.e. different gallium contents) are compared. Figure 22 shows calculated efficiencies of modules made from absorbers with different bandgaps, where cells made from the same material would have equal efficiencies. As can be seen in this graph, the benefits of increased absorber bandgap (i.e. increased gallium content) are both an improved maximal module efficiency for the same CIGS quality as well as a greater tolerance to variations in the ZnO:Al front contact conductance. The alternate way to take advantage of the higher bandgap is to use wider segments and thus less scribing rather than thinner, less conductive ZnO:Al. Any desired combination of the two is also possible.

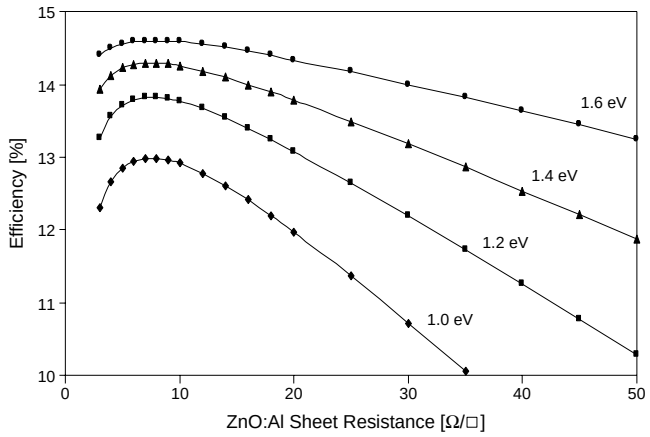

Figure 22. Calculated efficiencies for non-laminated mini-modules with 5 mm segment widths, made with CIGS absorbers with different bandgaps (i.e. different gallium contents) but equally efficient 16% ideal cells.

As discussed above, a higher voltage can be achieved by increasing the gallium content of the absorber. However, equal quality CIGS for all values of the bandgap are not achieved in practice. As shown in Figure 23, results sampled from different research groups using various absorber growth processes indicate that the increase rate of the open circuit voltage, $d(qV_{oc})/dE_g$, falls significantly for bandgaps greater than 1.2 eV [60]. This, in conjunction with a corresponding drop in fill factor with increasing gallium content, makes reported efficiencies drop considerably for bandgaps above 1.3 eV. Based on analysis of dark and light current-voltage measurements and voltage dependent quantum efficiency measurements, this decrease in fill factor and the relative voltage decrease with increasing gallium content has been explained by a voltage dependent current collection due to shortened diffusion length of minority electrons in the absorber, as well as enhanced recombination due to increasing defect density [61]. Strategies to achieve high performance at high voltages include bandgap grading (non-uniform composition) [62] and addition of sulfur to the absorber material [63].

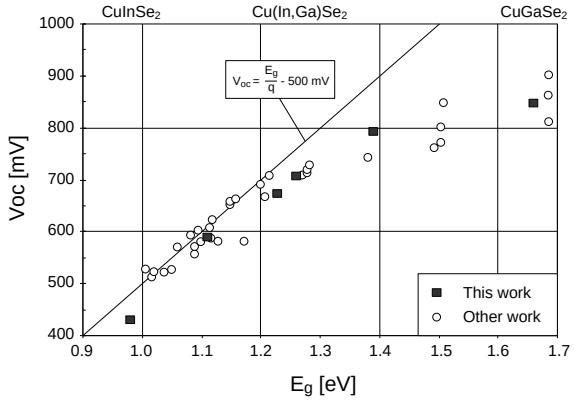

Figure 23. Open circuit voltages (V_{oc}) of Cu(In,Ga)Se_2 solar cells with different gallium contents prepared in various research labs using different growth processes. After [60].

From the relationship between cell performance and gallium content, optimized module parameters for each gallium content show that the expected discrepancy between cells and modules should decrease as the bandgap increases. Therefore, the gallium content for maximal module efficiency is higher than for maximal cell efficiency. Furthermore, it is more advantageous to be above this optimal value rather than below it. Higher gallium contents correspond to superior module designs in that they use less scribes and thinner ZnO:Al, both resulting in lower production costs.

5 Photovoltaic modules for low-concentrating systems

The high cost of photovoltaic energy has stimulated research on ways to increase performance of photovoltaic systems, for example by developing cheap and reliable booster reflectors or concentrating optics with the purpose of increasing radiation onto the collector surface. The use of sunlight concentrating devices in solar cell applications provides higher power output per illuminated cell area, and may, if cost of the concentrating device per unit area is much less than that of solar cell modules, lower electricity production costs. Despite that the art of concentrating light is complicated, in particular for applications requiring uniformity over large areas, several studies have indicated that the investment cost per annually delivered kWh of photovoltaic electricity can be significantly reduced by the use of low-concentrating reflectors [33, 64]. However, high-intensity illumination of solar cells implies a number of difficulties such as temperature effects and series resistance losses, which must be accounted for in designing the system [65]. The technical and physical aspects on photovoltaics for low-concentrating systems have been reviewed in Paper V, and different designs of CIGS modules for these conditions are discussed in Paper IV. Furthermore, a low-concentrating system with commercially available CIGS modules is evaluated in Paper VI. This work is briefly reviewed in the following sections.

5.1 Concentrating optics

Use of solar concentrating elements stretches way back in history. One of the earliest examples is the widespread story of how Archimedes in 212 B. C. repelled the Roman fleet when attempting to invade Syracuse, by means of concentrating the solar rays to a point where the enemy ships could be burned from a distance [66]. Whether this story has some truth to it or not has been debated since, but it is known that Archimedes already before the invasion had written the book “On Burning Mirrors”, which indicates that he possessed the necessary knowledge of the science of optics. Unfortunately, no copy of this book has survived to give evidence. Archimedes himself was killed less than a year later when Syracuse finally fell to land attack.

Concentration of light can be achieved with imaging or non-imaging optics. While imaging optics is used to transform light in an ordered way, for example to a focal point by the use of a glass lens or a parabolic mirror, non-imaging optics is used for transforming a radiation flux from one area to another where the paths of the individual light rays are of less importance [67]. In case imaging concentrators are used for solar energy applications, they have to follow the sun’s movement in the sky. This concept facilitates very high concentration ratios, and the photovoltaic modules for use with such devices have to be designed to allow high illumination levels. With non-imaging optics it is possible to design a device that concentrate the radiation from a certain angular region of the sky onto the receiver. Both the direct radiation and part of the diffuse radiation will be transferred to the receiver. These kind of systems can be stationary or change tilt angle only a few times per year to optimize performance.

The optics for solar concentrators can also be classified as either point focusing or line focusing. Point focus systems have circular symmetry and require two-axis tracking of the sun. These systems are used for achieving high concentration ratios. Line focus systems have cylindrical symmetry and are typically used in applica-

tions with moderate concentration ratios. Line focus systems require tracking around only one axis (if any).

In the present work, two types of non-imaging concentrators for use in photovoltaic systems are considered; the compound parabolic concentrator and the planar booster reflector.

5.1.1 Compound parabolic concentrators

The concept of the compound parabolic concentrator (CPC) is described in detail in [67]. The CPC consists of two reflective parabolas that funnel the radiation from the aperture to the receiver, as illustrated by Figure 24a. The angle $\theta_{a/2}$ is called the acceptance half-angle of the concentrator. All radiation incident with an angle of incidence $\theta \leq \theta_{a/2}$ will be transmitted through the concentrator, while radiation with $\theta > \theta_{a/2}$ is rejected by the concentrator. This is shown by the solid line of the angular acceptance function in Figure 24b. If the concentrator is truncated (for example by cutting through the dashed line in Figure 24a), the concentration ratio, defined as the area of the opening divided by the area of the receiver, will decrease. As a result, a fraction of the radiation reaching the entrance aperture with angles of incidence θ greater than the acceptance half-angle will reach the exit aperture directly, as indicated by the dashed line in the angular acceptance function. This is often a practical choice, since truncation of a CPC results in a substantial decrease in reflector area but only a small reduction in concentration.

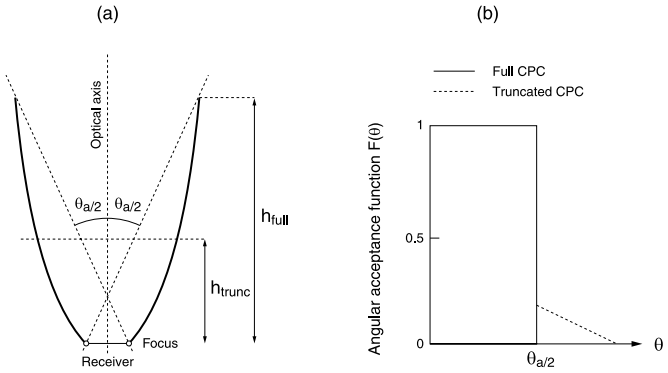

Figure 24. Cross-section of a compound parabolic concentrator (a). Angular acceptance function for a full and truncated CPC (b).

If the compound parabolic concentrator is designed to be stationary with a good all-year-around performance, an acceptance half-angle of about 30° is desirable, resulting in a concentration ratio of 2 [68]. However, if the tilt of the concentrator is changed 2–8 times per year, the acceptance angle can be chosen smaller to obtain higher concentration ratios of up to 4 [69].

The CPC is a line focus system, and the irradiance distribution over the area of the receiver is non-uniform. For a CPC designed for a concentration ratio of 4, there can, in a worst case, be areas on the receiver where the irradiance is up to 50 times higher than the irradiance without concentrators. In reality, the irradiance on the receiver is rarely higher than 3000–5000 W/m^2 [70]. Nevertheless, if CPCs are to be used in photovoltaic systems it is important to use photovoltaic modules that

are designed specifically for these conditions in order to get a satisfying system performance. This is further discussed in Paper V and experimentally verified in Paper VI.

5.1.2 Planar reflectors

With a planar booster reflector, the irradiation distribution on the receiver will have higher uniformity than for parabolic reflectors. A fundamental drawback, however, is that lower concentration ratios are obtained than for parabolic reflectors. Typically, the concentration ratios are at the 1.5 level. Calculations based on Swedish insolation data show that the annual output from photovoltaic module could increase in the order of 20–25% by using stationary external reflectors. With 2–8 annual adjustments of the booster reflector tilt, the annual irradiation can increase up to 40%, compared to a stationary photovoltaic module without reflector. This is further discussed in [71].

A photovoltaic system with a planar reflector under testing at the laboratories of Vattenfall Utveckling AB in Älvkarleby, Sweden, is shown in Figure 25. In addition to increasing the irradiance onto the photovoltaic module, the reflector here provides good snow protection.

Figure 25. Added value of planar reflectors. The picture shows a photovoltaic system with two modules, one with and one without a planar booster reflector. In addition to increasing the irradiance, the planar reflector provides good snow protection. The system is being tested in Älvkarleby, Sweden. Courtesy Björn Karlsson, Vattenfall Utveckling AB.

5.2 Characteristics of photovoltaic devices at high light intensities

Commercially available photovoltaic modules, whether based on crystalline silicon or any thin film technology, are usually designed for normal operating conditions (i.e. AM 1.5, 25 °C). When operated under high-intensity illumination in reflector systems, the technical and physical requirements on the devices are somewhat different, both on the module and on the cell level. For any choice of photovoltaic technology it is necessary to address these issues when designing the system in order to achieve good performance and cost effectiveness.

5.2.1 Non-uniform illumination

Conventional crystalline silicon modules are generally more sensitive than thin film modules to non-uniform illumination. For most crystalline silicon modules, the cells are series connected in several strings. Like for all types of modules with series connected cells, the module current is dictated by the cell with the lowest current generation. Hence, module performance will be limited by the output of that cell. In order to avoid this problem, crystalline silicon modules can be fabricated with one single row of series connected cells, as shown in Figure 27 below, or with rows of series connected cells connected in parallel. This requires, however, that the modules are custom designed, which in most cases is associated with higher costs.

The effects of non-uniform illumination are similar for thin film modules, but with the fundamental difference that all cells for this technology can span across the full width of the module. Thus, for a thin film module, the cells are series connected geometrically as well as electrically, and if the geometry of the non-uniformity is one-dimensional, the module can be oriented in such a way that all cells are illuminated with the same average intensity. The current generation will then be equally affected for each cell, and the power output will be determined by the average light intensity. This is further discussed in Paper V, where the effect of partial shading of a Siemens ST5 CIGS-based module has been studied. Here it is shown that the short circuit current and output power are reduced in proportion to the shaded area, while no significant change in fill factor is observed. A small difference in open circuit voltage is observed, and explained by the fact that the open circuit voltage is logarithmically dependent on the generated current [72].

5.2.2 Effects of temperature and light intensity

Typically, the conversion efficiency for each cell in a crystalline silicon module is around 15%. Since most of the remaining 85% of the energy in the incident light will be dissipated as heat in the solar cell, high intensity illumination will result in a considerable temperature increase, which will have an overall negative effect on the conversion efficiency. In addition, the device will experience increasing ohmic losses at high light intensities, which may also be crucial to device performance.

The temperature dependence of the conversion efficiency can be interpreted in terms of the individual temperature dependencies of the open circuit voltage, the short circuit current and the fill factor. The dominant cause of conversion efficiency degradation is the open circuit voltage dependence of temperature. The principal factor leading to the V_{oc} decrease is the associated increase in intrinsic carrier concentration. The minority carrier properties and, to a lesser extent, the photon absorption properties, are also affected. The physics behind these processes is thoroughly described in [72].

Ideally, V_{oc} is approximately linearly decreasing with temperature according to

$$\frac{dV_{oc}}{dT} = -\frac{E_{g0}/q - V_{oc} + \gamma(kT/q)}{T}$$

where E_{g0} is the linearly extrapolated zero temperature bandgap, and γ is a factor determining the temperature dependence of the diode saturation current. Substituting values for silicon, this would give an open circuit voltage decrease of 2.3 mV per °C [72].

The short circuit current is generally not strongly temperature dependent but tends to increase slightly with increasing temperature. This can be attributed to increased light absorption, since the bandgap decreases with temperature. Results from simulations indicate that I_{sc} for the crystalline silicon cells studied in [73] increases in the order of 9 mA or 0.25% per °C at a light intensity of 1000 W/m^2.

If parasitic resistance effects are neglected, the fill factor *FF* is temperature dependent only through the open circuit voltage. For silicon, the empirical expression for the fill factor is

$$FF = -\frac{v_{oc} - \ln(v_{oc} + 0.72)}{v_{oc} + 1}$$

where v_{oc} is the normalized voltage, defined as

$$v_{oc} = \frac{V_{oc}}{kT/q}$$

In [73] the fill factor decrease for silicon cells is estimated to approximately 0.2% relative per °C at a light intensity of 1000 W/m^2.

The resulting overall efficiency decrease due to elevated operating temperature, taking the temperature dependencies of V_{oc}, I_{sc}, and *FF* into account, will be in the order of 0.4–0.5% relative per °C [72].

For concentrator systems, the module conversion efficiency determines the area of the concentrator required for a given system power output. Therefore, it is important to achieve as high module efficiencies as possible. For an ideal solar cell, that is a solar cell with negligible shunt and series resistance, it can be shown that $I_{sc} \propto G$ and $V_{oc} \propto ln(G)$, where G is the incident light intensity [72], and that the conversion efficiency η is given by

$$\eta = \frac{FF \cdot I_{sc} \cdot V_{oc}}{G}$$

Assuming that the fill factor is not affected by the light intensity, the conversion efficiency will thus increase logarithmically with increasing light intensity. In reality however, the effect of non-negligible series resistance and high current levels may well lead to reduced conversion efficiencies.

The effects of temperature and series resistance for a crystalline silicon cell at two different light intensities are demonstrated in Figure 26. The curves are calculated using the two-diode model further described in [65], and the efficiencies are normalized to one at a temperature of 25 °C (298 K). As can be seen, the impact of the series resistance is greater at higher temperatures and intensities. This emphasizes the importance of keeping the series resistance at a low value for concentrator applications.

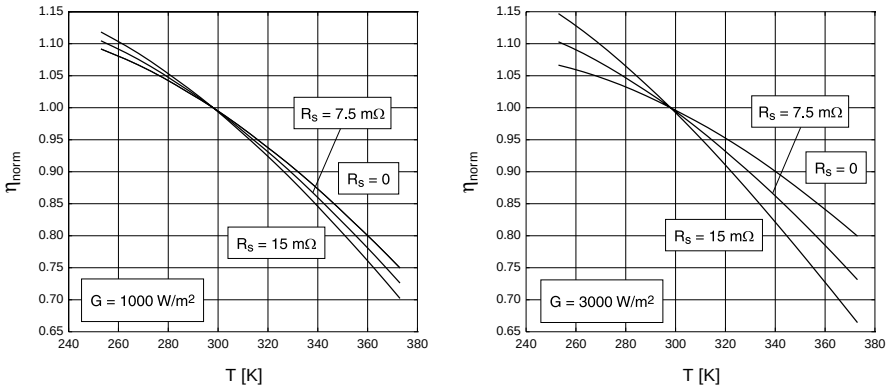

Figure 26. Calculated effects of temperature and series resistance for a crystalline silicon cell at different light intensities. The efficiencies are normalized to one at a temperature of 25 °C (298 K) for all values of the series resistance. The model and input data used are further described in [65].

It is further shown in Figure 26, that the temperature dependence of the low series resistance cell is relatively stronger at low light intensity, while the opposite is true for the high series resistance cell. At low series resistances, the parasitic ohmic losses are small and the V_{oc} is the dominant efficiency-limiting factor. Ideally, the V_{oc} decrease is linear with temperature, and not depending on light intensity. However, while the V_{oc} temperature dependence is not affected, the V_{oc} itself increases logarithmically with light intensity, yielding a slightly higher V_{oc} and thus relatively weaker temperature dependence of the efficiency. For high series resistances, again, the parasitic losses become a critical efficiency-limiting factor, which results in a stronger temperature dependence [65].

5.2.3 Crystalline silicon modules for low-concentrated light

The impact of high temperatures and light intensities, as well as effects of non-uniform illumination, have been studied experimentally in [74], where crystalline silicon modules are used in a water-cooled hybrid system with low concentrating aluminum compound parabolic concentrators. The system consists of three rows of collectors. In each row there are four 12-cell single-string photovoltaic modules which are cooled by water circulating in a cooling fin glued onto the back of the modules. The modules are composed of conventional 10×10 cm^2 single-crystalline silicon cells. The geometrical concentration ratio of the compound parabolic concentrators is 4, with an acceptance half-angle of 12°. The reflectors are fabricated of bright anodized aluminum and truncated to a height of 45 cm. An overview of the system and a detail of the crystalline silicon module are shown in Figure 27. The system is evaluated in detail in [74], but some qualitative aspects on its performance are briefly discussed in the following.

The geometry of the concentrator has an observed impact on the electrical performance of the system. There is a pronounced focal line with significantly higher light intensity along the string module. This line traverses the module as the sun moves across the sky during the day. The presence of this line of high local concentration, particularly at incidence angles near the half acceptance angle, causes a non-uniform current generation across the area of the cells, which may

result in severe loss of electrical performance. The tilt of the concentrator determines the position of the focal line, so, to achieve best all-day-around performance it is important to find the optimal tilt angle. For an efficiently cooled module, with a low series resistance, the maximum output is expected when the focal line is in the middle of the cells, between the conducting fingers [71].

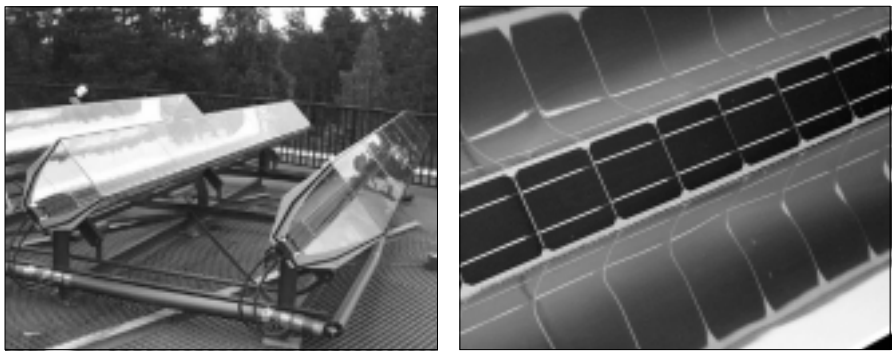

Figure 27. A hybrid photovoltaic/thermal system equipped with low-concentrating CPC collectors. The system is installed at Vattenfall Utveckling AB in Älvkarleby, Sweden. Further details on this system are given in [74].

Although the geometrical concentration ratio of the reflectors is 4, the short circuit current of the modules is observed to increase only by a factor of 2.7 as compared to a reference module without reflectors. This is partly due to the optical efficiency of the concentrator, and partly due to the non-uniform illumination, which reduces the effective concentration ratio [75]. At noon, when the system should exhibit its maximal power output, series resistance and temperature effects causes the fill factor and voltage of the modules to decrease, which results in an electric power output about a factor 2.2 higher than without reflectors. This result further emphasizes the importance of using modules with low series resistance and efficient cooling.

5.2.4 Characterization of a Siemens CIS module in a concentrating system

As part of the work on CIGS modules for low-concentrating applications, a prototype system with parabolic aluminum reflectors for wall integration (see Figure 28) has been evaluated (Paper VI). The system is designed for the $Cu(In,Ga)Se_2$-based Siemens ST5 thin film module, as a ready-to-use wall element with an insulating backside, and is intended to substitute a part of a south-facing wall. The height of each cell and reflector segment is 55 cm. The focal length of the parabola is 15.4 cm. The ST5-module, which measures 20.6 cm by 32.8 cm including the aluminum framing, is tilted forwards by 20° relative to the horizontal plane and by 45° relative to the optical axis of the parabola.

Tests of the system have been carried out both outdoors in sunlight and indoors using the large-area solar simulator described previously (see section 3.4.1). The electrical performance of the system has been tracked as a function of module temperature and the effective solar height (Paper VI), and has been compared to results obtained from optical modeling [76].

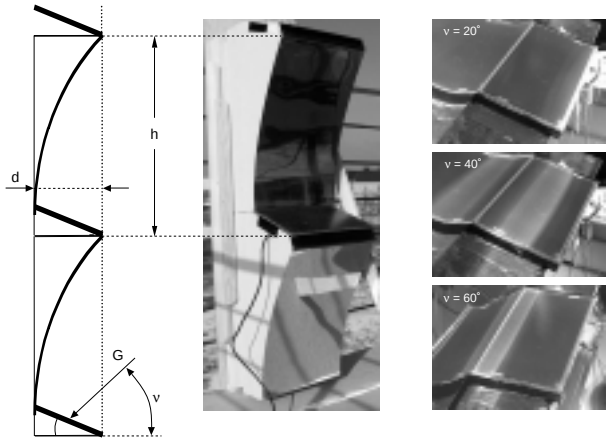

Figure 28. A prototype of a concentrating element for wall integration at high latitudes. The parabolic reflector has a concentration ratio of 3. G is the incoming irradiation and v is the effective solar height. The Siemens ST5 photovoltaic module is tilted forwards by 20°. The depth d of the wall element is 180 mm and the opening of a single concentrating element h is 550 mm. The illumination on the module is non-uniform, due to the parabolic reflector, and the lateral position of the focal line changes with the effective solar height.

Figure 29 shows the results from indoor and outdoor measurements of the electric power output at different effective solar heights. As a comparison, results from measurements without concentrating elements are shown. The higher open circuit voltage for the indoor measurements is due to better control of the module temperature. The geometric concentration ratio of the system is 3, but the maximum power output from the modules is only 1.9 times that of identical vertical modules without reflectors. This is due both to optical losses and a decrease in fill factor under concentrated illumination. The fill factor drop is explained by ohmic losses in the front contact of the module and by high cell temperatures resulting in a lower open circuit voltage.

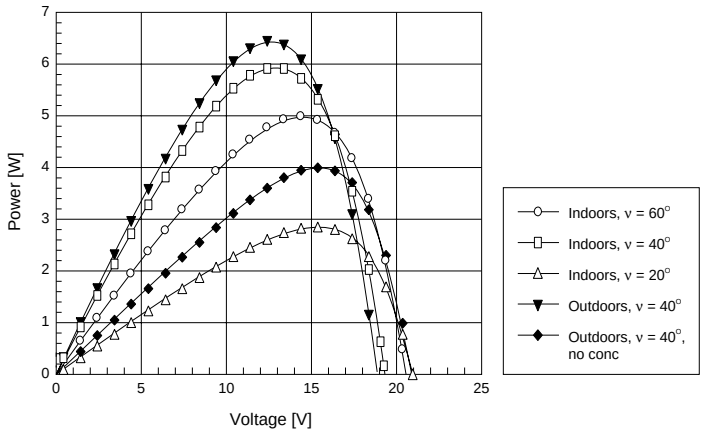

Figure 29. Measured power as function of voltage for different effective solar heights, v, for a Siemens ST5 photovoltaic module.

As can be seen in Figure 28, the illumination on the module is non-uniform and the lateral position of the focal line changes with the effective solar height. A solar height of about 40° is found to give the highest electric output, and the optical efficiency of the system at this solar height has been determined from measurements of the short circuit current to approximately 75%. The non-uniform illumination will furthermore give large temperature gradients within the module. At a solar height of 25°, the temperature, as measured by a surface temperature probe, close to the parabolic reflector was 40 °C, while it was 120 °C in the focal line [76]. The impact of these large temperature gradients on the system performance needs to be further investigated.

The wall element is a technically attractive alternative for building integration at high latitudes. However, in order to meet the expectations on economical viability, the system must be sufficiently cooled and the modules used should be of thin film type and designed for high intensity illumination.

5.3 Design, fabrication, and testing of gridded CIGS modules

From a geometrical point of view, the conventional off-the-shelf crystalline silicon modules are not suitable for use with parabolic reflectors. This is because these type of reflectors give non-uniform illumination across the surface of the receiver, as has been discussed above. To avoid this problem, the hybrid system described previously uses specially designed, single-string modules. A better choice would be to use modules based on any of the thin film technologies. In Papers IV and V, the design and fabrication of a CIGS thin film module is discussed. Here, the detrimental resistive losses in the front contact at high light intensities are avoided by assisting the front contact with a metal grid. Also at one-sun operation, gridded modules can be advantageous, and this not only to achieve better performance. More important are the benefits of improved window processing tolerance and throughput, as well as improved degrees of freedom of the module geometry. The basic ideas for looking at the use of metal grids in modules are that

- the stringent requirements on the front contact conductance can be eased leading to the use of much thinner (i.e. cheaper) front contact deposition;
- the cell segment width is no longer imposed by the front contact quality, and therefore, much wider segments are possible, which gives a higher degree of freedom in the choice of total module voltage;
- the interconnect scheme can be simplified and result in less complex scribing and less dead area;
- there is a potential for low concentration applications.

In its simplest form, the gridded module is based on a standard interconnect structure, where the grid is only assisting the front contact. A slightly more sophisticated design is that when the grid is used to connect to the molybdenum back contact of the consecutive cell. In the latter case all mechanical scribing is performed after front contact deposition, and lower resistive losses as well as improved stability (see section 6.4) can be expected.

Design of CIGS modules for 1-sun conditions, and in particular optimization of the ZnO:Al front contact, has been discussed above. For a gridded module the matters of design and optimization are somewhat different. With this design, the current is collected by the grid and flows in the gridlines along the cell to the inter-

connect. Cell width is therefore no longer limited by the front contact conductance, but by resistive grid losses. Provided that the grid design is such that these losses are small, a high degree of freedom of the module geometry is obtained. All gridded modules considered in the present work have a grid composed of a 50/3000/50 nm thick Ni/Al/Ni sandwich with an aluminum bulk resistivity of 4 μΩcm, similar to that of baseline test cells (see section 3.2.6). Thus, the grid design parameters are limited to line width and spacing.

Figure 30 shows the tolerance to variations in ZnO:Al front contact conductance for various module designs. Here, as in section 4.3.2 (Figure 21), the calculations of module efficiencies are based on the characteristics of a baseline cell with an active area efficiency of 14.4% at normal operating conditions.

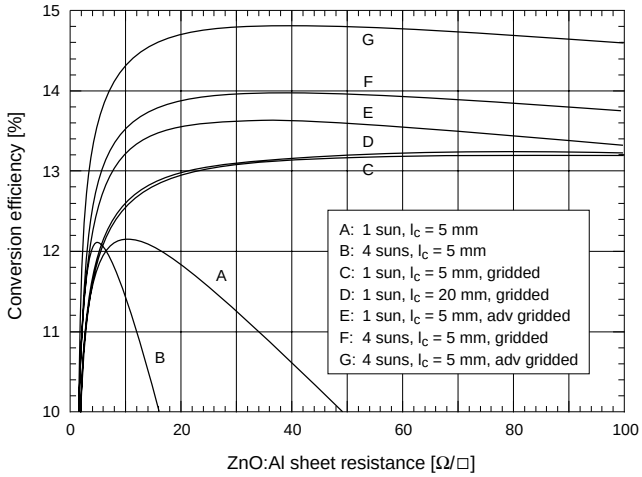

Figure 30. Calculated conversion efficiencies relative to varying ZnO:Al front contact conductivities for different module designs at 1- and 4-suns illumination.

Curve A represents an optimized design of a conventional module (cf. section 4.3.2). With this design, variations in performance are relatively small at 1-sun illumination. Assuming that a 5% relative decrease from maximum efficiency is acceptable, the sheet resistance of the ZnO:Al can be chosen within a wide range. However, when this design is applied to a module operating at 4-suns illumination in a system with low-concentrating reflectors (as shown by curve B), a much narrower process window is allowed in order to avoid resistive losses caused by the higher current density. Furthermore, the shift in optimum ZnO:Al sheet resistance from 10 down to 5 Ω/□ nearly doubles the current loss (normalized to 1-sun illumination). As a result, the expected efficiency gain due to the logarithmic dependency of open circuit voltage on light intensity does not occur. Therefore, at 4-suns illumination, a gridded design is recommended. As shown by curve F, both the efficiency and the tolerance to process variations are greatly enhanced. Optimization of the grid is a matter of trade-off between improved current collection and shadowing and resistive losses imposed by the grid.

The gridded design may be advantageous also at 1-sun illumination. In order to reduce cost of the front contact it is desirable to have a high-throughput deposition

process. For the baseline, throughput can be improved by reducing film thickness. But since this will also have an impact on the electrical properties, it is necessary to assist the front contact with a grid. A module with such a design, based on the standard interconnect structure, is represented by Curve C. As can be seen, this module exhibits a higher efficiency as well as better tolerance to variations in the front contact process.

For commercially available modules, the cell length would be strictly defined within boundary conditions imposed by the process equipment and the required output voltage. As a consequence, these modules would rarely have optimal performance. With a gridded design, however, the choice of cell length is more flexible as illustrated by Curve D where a module with 20 mm wide segments is simulated. In this case, the performance is similar to that of the 5 mm gridded design in Curve C, which indicates that the higher resistive and shadowing losses here are balanced by the relatively lesser interconnect dead width.

The gridded module design also enables the use of more advanced interconnect structures. This study includes a design based on a recently developed advanced interconnect, which relies on a sophisticated back contact pattern design. With this structure, the interconnect via (P_2) can be performed in points and the isolation scribe (P_3) can almost completely coincide with the cell definition scribe (P_1). This structure enables a simplified scribing sequence, where the total dead width of the interconnect is reduced to less than 100 μm, resulting in significantly lesser area loss. Curves E and G show the calculated performance for modules based on the advanced interconnect structure, at 1- and 4-suns illumination respectively.

Figure 31 presents the current world record efficiency for thin film modules of 16.6% at standard test conditions, as confirmed by Fraunhofer Institut für Solare Energiesysteme, Freiburg, Germany. This 16 cm^2 encapsulated mini-module is fabricated with a thin transparent front contact that is complemented by a metal grid.

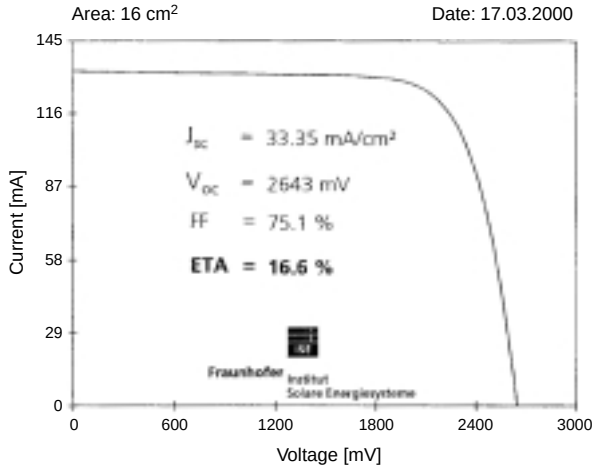

Figure 31. I-V characteristic of the current world record efficient CIGS mini-module, measured under standard test conditions by the Fraunhofer Institut für Solare Energiesysteme. This device is encapsulated and consists of four 1 cm wide segments. It uses grids for enhanced current collection.

In line with the previous discussion, a CIGS mini-module for low-concentrated illumination has been designed and fabricated on a 5×5 cm^2 soda-lime glass substrate (see Figure 32). In this work, all utilized process steps are within the frames of the baseline as previously described. The module is composed of nine 5×45 mm^2 segments, which are monolithically series integrated using the standard interconnect structure (cf. section 3.2.6). The width of each interconnect is approximately 300 μm, resulting in 6% area loss. The ZnO:Al front contact has a sheet resistance of 40 Ω/□, corresponding to a thickness of approximately 150 nm.

Figure 32. A gridded CIGS module, designed for low-concentrated illumination.

Current collection in the front contact is enhanced by 50/3000/50 μm thick, 100 μm wide, and 4.5 mm long Ni/Al/Ni grid fingers, with a spacing of 2.5 mm. The maximum lateral current collection length is thus 1.25 mm. The additional area loss due to grid coverage is 4%, while ohmic losses in the gridlines are causing an approximate 1% power loss at 1-sun light intensity and close to 5% at 4 suns. The device is encapsulated using a 1 mm thick low-iron cover glass with EVA as encapsulant. Current-voltage and power characteristics of the 4X module at 1- and 4-suns illumination are shown in Figure 33.

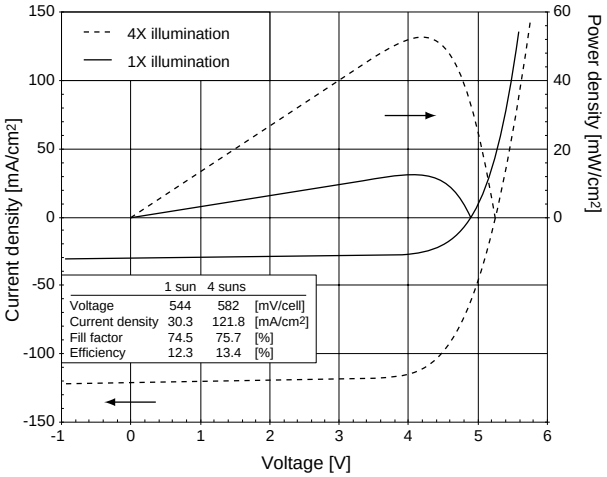

Figure 33. Current-voltage and power characteristics of a 4X CIGS module, measured at 1- and 4-suns illumination using a solar simulator.

These measurements are obtained using a solar simulator. In order to avoid temperature effects, the measurements are performed within a timeframe of less than a second. As can be seen, both voltage and fill factor are increasing under high-intensity illumination. This is in good agreement with theory [72].

In Table 1, the calculated effects of some loss mechanisms are compared for the 4X-module and a conventional module under 4-suns illumination. This assumes an active area efficiency of 16% at a light intensity of 400 mW/cm^2. The difference in ZnO:Al conductance is clearly reflected in both the optical and ohmic losses of the front contact. Due to the thinner ZnO:Al used for the gridded module, the optical losses are cut down to ⅓. Thinning down the front contact will, however, lower its conductance. Nevertheless, the ohmic losses can be significantly reduced since the lateral current collection is only ¼ of that of a conventional baseline module.

	Conv. design	4X design	
Interconnect dead area	3.8	3.8	[mW/cm^2]
Grid shadowing	-	2.6	[mW/cm^2]
Grid ohmic	-	0.3	[mW/cm^2]
Front contact optical	0.9	0.3	[mW/cm^2]
Front contact ohmic	11.0	2.6	[mW/cm^2]
Others	2.4	0.6	[mW/cm^2]
Total	18.1	10.2	[mW/cm^2]

Table 1. Losses of a conventional and a 4X CIGS module, calculated at 4-suns light intensity.

A gridded module design has several technical advantages over conventional modules, both with concentrated illumination as well as in standard applications. Less inactive area, higher front contact process tolerance and improved degrees of freedom of the module geometry are factors enabling fabrication of better performing modules. The freedom in the segment widths also translates to a freedom in the current to voltage output of the full size modules. Furthermore, a gridded design will facilitate low-cost front contact fabrication. The technical advantages are strong arguments for gridded modules. However, it is left to be proven that the grid technology is realistic in production, and that the benefits of this concept overweigh the cost of grid deposition. Since that is beyond the scope of this thesis, it can only be pointed out at this time that the synthesis and manufacturing issues discussed reflect back directly on production costs.

6 Long-term stability of CIGS-based devices

Long-term stability is of crucial importance for CIGS based devices to become a commercially viable product. Although outdoors testing of encapsulated modules have demonstrated good stability, in some cases for several years [17, 54], it is well known that standardized accelerated tests, like the IEC 1646 damp heat test [77], often cause severe degradation [32, 78].

In the present work, accelerated lifetime tests have been carried out in damp and dry heat conditions on a large number of devices (Papers I, II, III, and VIII). While damp heat exposure is proven to be harmful to CIGS devices – encapsulated as well as bare – several studies on dry heat testing demonstrate no or very little impact on performance [32]. This indicates that humidity is a primary catalyst to the mechanisms involved in the degradation process. It is therefore likely to believe that enhanced stability could be achieved simply by improving the encapsulation technology, which has also been confirmed experimentally [79, 32]. However, it would be rash to accept this as a universal solution to the stability issue. The fact that very little is known about the complex solid state chemistry of the ZnO:Al/ZnO/CdS/Cu(In,Ga)Se_2/Mo/Glass structure of CIGS devices raises concerns about undesired chemical reactions in the long run [80]. Hidden long-term issues, such as diffusion of impurities, the action of humidity, or other subtle degradation mechanisms, will still require attention.

Further enhanced understanding of the mechanisms involved in device degradation is needed, and this need is becoming increasingly urgent as the CIGS technology is emerging towards large-scale production.

6.1 The IEC 1646 qualification standard

The IEC 1646 thin film module qualification standard [77] comprises a number of test procedures. These include visual inspection, insulation test, and performance tests at various light- and temperature conditions, as well as various endurance tests like the damp heat test, thermal cycling test, hot-spot endurance test, UV test, and a humidity-freeze test. In addition, modules should pass various mechanical endurance tests, like the mechanical load test, twist test, hail test, and robustness of terminations test. According to the qualification standard, a module design shall be judged to have passed the qualification tests, and therefore to be IEC type approved, if the tested sample meets all the following criteria:

- the degradation of maximum output power at standard test conditions does not exceed the prescribed limit after each test;
- after the final light soaking, the maximum output power at standard test conditions is not less than 90% of the minimum value specified by the manufacturer;
- no sample has exhibited any open circuit or ground fault during the tests;
- there is no visual evidence of a major defect;
- the requirements of insulation and wet leakage current tests are met.

If two or more modules out of eight do not meet these test criteria, the design shall be deemed not to have met the qualification requirements [77]. In the present work, the emphasis is mainly put on the damp heat test, since humidity penetration into the module encapsulation is believed to be a major cause of failure in accelerated

lifetime tests of CIGS-based devices. The purpose of the damp heat test is to determine the ability of the module to withstand the effects of long-term penetration of humidity. The test procedure is as follows:

- *preconditioning*. Before conducting the test, the module shall be annealed.
- *testing*. The following conditions are applied:
  - test temperature: 85 °C ± 2°C
  - relative humidity: 85% ± 5%
  - test duration: 1000 h
- *recovery*. The module shall be submitted to a recovery time between 2 and 4 hours.

The pass criteria for the damp heat test are the following:

- No evidence of major visual defects.
- Insulation resistance shall meet the same requirements as for the initial measurements.
- The degradation of maximum output power at standard test conditions shall not exceed 5% of the value measured prior to the test.

According to a recent study on procedures for performance measurements and lifetime testing of thin film photovoltaic devices [81], the IEC 1646 qualification standard is to a large extent just transferred from that of crystalline silicon modules. It is adapted especially for the amorphous silicon module technology, for which it is rather adequate. For other thin film technologies, however, there are several parts of the standard that should be reconsidered. Further details on this are given in [81], but the conclusion is that the relevance of the IEC 1646 standard procedures can and should be questioned. However, even if standards are redefined to take into account the special character of thin film modules, the modules still have to withstand harsh and humid conditions in real outdoor climates. Thus, it is important to understand the mechanisms involved in module degradation, and to solve the current stability problems.

6.2 CIGS modules in field testing

Field testing is of course the most accurate method to recognize relevant degradation mechanisms in photovoltaic modules. However, in order to be viable, the field tests have to be true long-term (20–30 years) and carried out on the ready commercial product. To speed up the ageing processes, various forms of accelerated tests are applied in parallel.

Many reports from long-term field testing of photovoltaic systems generally point out the modules – almost all made using wafer-based silicon cells – as the most durable part of the systems. Failure rates as low as one per 10 000 per year are an important achievement for the wafer-based silicon technology. For thin film technologies, the picture is somewhat less clear but yet promising. The thin film solar cell technology that was closest to commercialization in the 1980s was based on copper sulfide, Cu_2S/CdS [14]. However, these devices soon proved to suffer from an electrochemical instability that led to degradation in performance [15]. Partly because of this problem, the copper sulfide technology was never released on the market. The first actually commercially available thin film technology,

amorphous silicon, also suffers from a serious degradation, in this case associated with exposure to light (see section 2.2.1). Despite many years of research efforts to overcome the problem, this is still what keeps the efficiencies of amorphous silicon cells below those of other thin films. Combined with some start-up problems with encapsulation and quality control, the poor outdoor performance of amorphous silicon devices has until recently defined the bad reputation of thin films. Today, amorphous silicon modules are marketed with stabilized efficiency figures, and the efficiencies have also improved as the devices are manufactured in tandem or triple junction structures.

The emerging thin film technologies CdTe and CIGS, have both shown good stability in various field tests. The data presented in Figure 34 result from extensive outdoors testing of CIS and CIGS thin film modules, performed by NREL (US National Renewable Energy Laboratory) [17]. This is a proof-of-concept that stability is possible. Other groups have shown similarly encouraging results, although over shorter periods of time [82, 83].

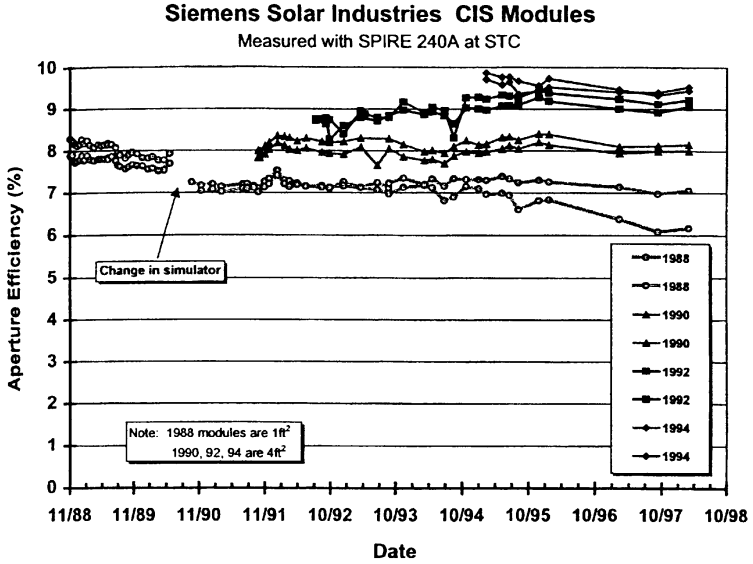

Figure 34. Results from outdoors long-term testing of 1×1-foot and 1×4-foot CIS modules at NREL. From [17].

A field testing effort has recently been initiated at the Ångström Solar Center. Figure 35 shows a photograph of the test site still under construction. Solar irradiation is measured both by a pyranometer and by a calibrated and temperature-compensated silicon sensor. The tested modules are operating at their maximum power points and data are captured using a data logger. The site is monitored in real-time by a computer. To date, one Siemens ST40 40-watt CIS module and one NESTE 100-watt multi-crystalline silicon module are tested. In addition, a first small 5×5 cm^2 ÅSC CIGS module has been mounted, although not connected to the maximum power point tracker, and tested for approximately 9 months, showing stable performance.

Figure 35. Field test site under construction at the roof of the Ångström Laboratory, Uppsala, Sweden. Courtesy Einar Söderman, Uppsala University.

6.3 Results from dry heat tests

Dry heat tests are performed in a low-pressure air atmosphere at 85 °C using a low-vacuum chamber with a temperature controlled hotplate. For reference purpose, dry heat tests are also carried out in argon atmosphere at 85 °C using a gas furnace.

Both cells and modules generally show stable properties in dry heat tests. Figure 36 shows results from an 8000-hour extended dry heat test (85 °C, argon atmosphere) of a non-encapsulated baseline cell.

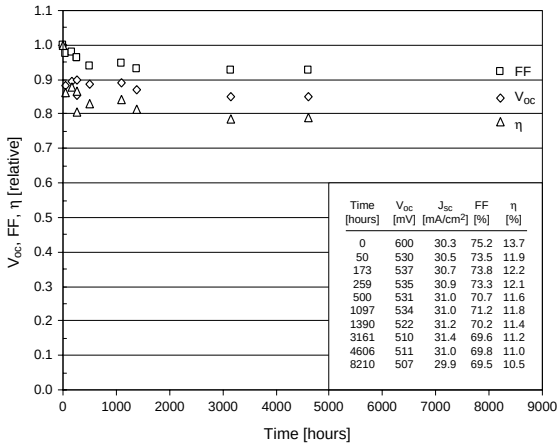

Time [hours]	V_{oc} [mV]	J_{sc} [mA/cm^2]	FF [%]	η [%]
0	600	30.3	75.2	13.7
50	530	30.5	73.5	11.9
173	537	30.7	73.8	12.2
259	535	30.9	73.3	12.1
500	531	31.0	70.7	11.6
1097	534	31.0	71.2	11.8
1390	522	31.2	70.2	11.4
3161	510	31.4	69.6	11.2
4606	511	31.0	69.8	11.0
8210	507	29.9	69.5	10.5

Figure 36. Dry heat test of a naked baseline cell using a gas furnace at 85 °C and argon atmosphere.

Both voltage and fill factor exhibit initial changes, but the performance stabilizes at approximately 80% relative to as-grown values after about 1500 hours. These initial fluctuations in voltage and fill factor are often observed, also in damp heat tests, and it is likely to believe that these are similar to the annealing effects

reported by many groups [84]. The small current variations seen are most likely due to lamp changes on the solar simulator (see section 3.4.1).

Figure 37 shows results from a 4000-hour extended dry heat test (85 °C, low-pressure air) of a naked and an encapsulated 4-segment mini-module. As can be seen in this graph, the encapsulated module exhibits some initial change in efficiency followed by a slow decay, mainly caused by small losses in fill factor. The non-encapsulated module is more stable initially but show an equally small long-term degradation. The initial performance drop of the encapsulated module is probably caused by thermal stress during the encapsulation process, where a temperature as high as 150 °C is applied for up to 30 minutes, depending on the type of lamination technology used (see section 3.3).

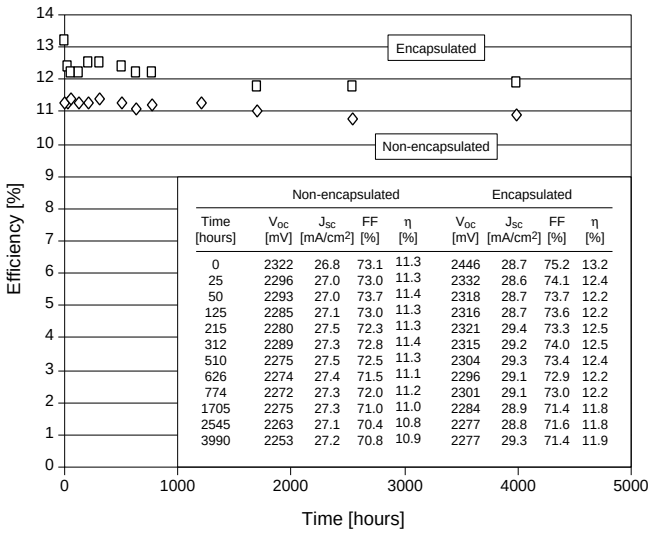

	Non-encapsulated				Encapsulated			
Time [hours]	V_{oc} [mV]	J_{sc} [mA/cm^2]	FF [%]	η [%]	V_{oc} [mV]	J_{sc} [mA/cm^2]	FF [%]	η [%]
0	2322	26.8	73.1	11.3	2446	28.7	75.2	13.2
25	2296	27.0	73.0	11.3	2332	28.6	74.1	12.4
50	2293	27.0	73.7	11.4	2318	28.7	73.7	12.2
125	2285	27.1	73.0	11.3	2316	28.7	73.6	12.2
215	2280	27.5	72.3	11.3	2321	29.4	73.3	12.5
312	2289	27.3	72.8	11.4	2315	29.2	74.0	12.5
510	2275	27.5	72.5	11.3	2304	29.3	73.4	12.4
626	2274	27.4	71.5	11.1	2296	29.1	72.9	12.2
774	2272	27.3	72.0	11.2	2301	29.1	73.0	12.2
1705	2275	27.3	71.0	11.0	2284	28.9	71.4	11.8
2545	2263	27.1	70.4	10.8	2277	28.8	71.6	11.8
3990	2253	27.2	70.8	10.9	2277	29.3	71.4	11.9

Figure 37. Dry heat tests of a naked and an encapsulated mini-module in low-pressure air at 85 °C.

6.4 Damp heat testing

In the present work, damp heat conditions are imposed by a Vötsch VC2020 climate chamber (see Figure 38) and the tests are extended over periods of up to 1000 hours. The test conditions are similar to the IEC 1646 international standard damp heat test recommendations, i.e. 85% relative humidity at 85 °C [77]. In order to extract information of degradation mechanisms possibly not seen otherwise, these already very harsh conditions are further accentuated by testing non-encapsulated samples.

Figure 38. The Vötsch VC2020 climate chamber used for accelerated ageing of CIGS and related devices.

6.5 Cell degradation

From damp heat tests it is observed that non-encapsulated CIGS devices degrade in both open circuit voltage and fill factor. After 4–500 hours, these parameters tend to saturate at a level 20–40% lower than initial values, resulting in a 40–60% performance loss. Figure 39 shows an example of the evolution of the current-voltage characteristics of a baseline cell during damp heat exposure.

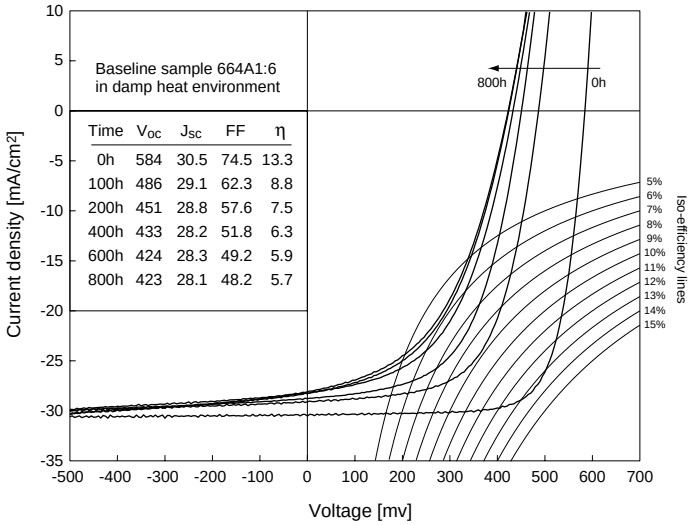

Figure 39. Evolution of the current-voltage characteristics of a baseline cell during extended damp heat exposure.

6.5.1 Voltage and fill factor

The causes of the voltage degradation have been only briefly investigated in this work, but the results discussed in Paper I are in line with those presented by other authors. Studies on oxidation of bare CIGS films at room temperature in the presence of humidity show that oxides of indium, gallium, and selenium, as well as the formation of elemental selenium are observed at the surface and in the bulk of the CIGS film, resulting in deteriorating electronic properties of ZnO/CdS/CIGS devices [47, 85]. In Paper I it is suggested that similar effects for complete devices exposed to damp heat conditions could be caused by water or oxygen diffusing in through the window. A correlation between the increased defect density and the degradation in open circuit voltage that is observed in [86] leads to the conclusion that the changes in the bulk or at the grain boundaries are responsible for losses in the open circuit voltage.

It has further been found that the oxidation of CIGS is accelerated in the presence of sodium [87]. In a humid atmosphere, a Na-O-CIGS complex is formed on the surface of the CIGS. This is an irreversible process which leads to a surface oxidation and hence a reduction of the amount of sodium from the CIGS surface and from internal surfaces and grain boundaries, and is expected to negatively influence the electronic properties of the CIGS [88].

The phenomenon of voltage degradation is believed to be dominated by the effect of enhanced recombination due to increasing defect density in the bulk and at the grain boundaries of the CIGS absorber, and by a shift of the Fermi level at the CIGS/CdS interface. In addition, the optical and electrical properties of the ZnO:Al transparent front contact are affected by damp heat exposure. The concentration of free carriers in the ZnO:Al will decrease with damp heat treatment, leading to increasing film resistivity. This could impact the fill factor of devices both in terms of higher ohmic losses in the front contact, and by imposing a shift of the built-in electric field towards the *n*-region of the *p*-*n* junction, which will raise the electron barrier at the CIGS/CdS interface [86]. In Paper III it is shown that additional voltage and fill factor effects occur in modules due to degradation of the interconnect between cells.

6.5.2 Current

Current is often not affected by accelerated ageing of baseline devices. As discussed in Paper I, the optical properties of the front contact in fact improve slightly with damp heat treatment. Nevertheless, in some cases, like in Figure 39, a significant drop in current is observed. Figure 40 shows quantum efficiency measurements of the baseline sample presented above. As can be seen in this figure, the largest drop occurs in the near infrared region, here in the 800–1200 nm wavelength interval. This indicates that recombination is the predominant mechanism of the current loss.

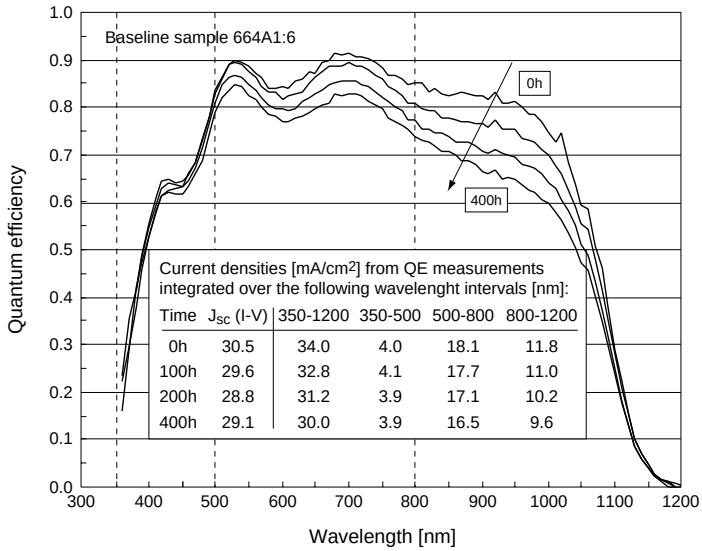

Figure 40. Quantum efficiency measurements of a baseline sample during accelerated ageing in damp heat conditions.

6.5.3 Influence of gallium

The influence of gallium on the long-term stability of CIGS devices has been investigated in a recent, not yet published work. In this work, a set of non-encapsulated $Cu(In_{1-x},Ga_x)Se_2$ solar cells have been fabricated with different gallium contents $x \equiv [Ga]/([Ga]+[In]) \approx \{0, 0.3, 0.4, 0.5, 0.6, 1.0\}$, and exposed to extended damp and dry heat conditions. The cell degradation is studied by temperature dependent current-voltage measurements (I-V(T), see section 3.4.2) at different stages of degradation. It is observed that all samples, except pure $CuGaSe_2$, are stable in dry heat conditions. After 1000 hours of damp heat exposure, the samples with gallium contents close to 0.4 show the smallest efficiency degradation of about 25% relative to their initial performance, while pure $CuInSe_2$ and the $CuGaSe_2$ samples exhibit the most severe degradation with performance losses of around 90% and 65%, respectively.

I-V(T) measurements of the samples in their initial state, prior to degradation, shows that the samples with $x \leq 0.5$ had forward currents dominated by tunneling enhanced recombination in the space charge region, while the pure $CuGaSe_2$ samples were limited by recombination at the CdS/absorber interface [60]. The analysis of I-V(T) measurements of the samples at different stages of their degradation shows that, for some samples, the activation energy of the dark current is lowered during degradation. One example of this is given in Figure 41, where the activation energies of a baseline cell ($x \approx 0.3$) have been calculated from I-V(T) measurements in both dark and light conditions, before and after 400 hours of damp heat exposure. Here, it is seen that the activation energy is lowered after degradation, and that the effect is strongest for the illuminated sample. While other authors have reported that recombination via defect states in the absorber layer is the dominant recombination mechanism before as well as after degradation [86],

the present observation of the decreasing activation energy can be correlated to a change from tunneling enhanced space charge recombination to interface recombination.

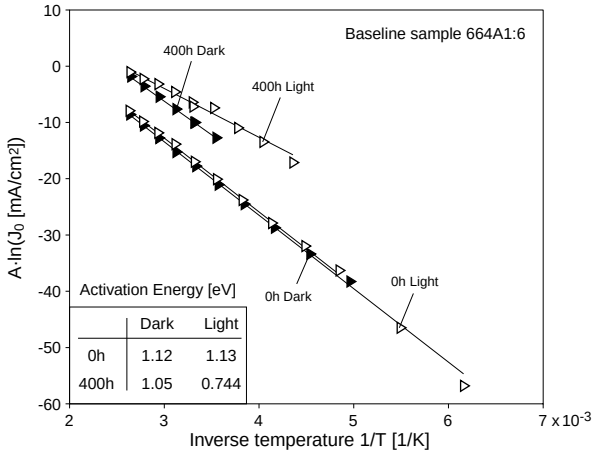

Figure 41. Activation energies measured for a baseline CIGS cell before and after 400 hours of damp heat exposure. The activation energies are given by the slopes of the lines, which are obtained from temperature dependent current-voltage measurements.

6.5.4 The grid

During accelerated ageing of baseline small-area test cells, it has shown to be important to protect the grid itself from corrosion in order to avoid artefacts in the test results. Originally in the baseline, a Ni/Al grid structure was used for test cells, but since this structure easily corrodes in the hot and humid environments, an improved grid was developed (see Paper I) that includes a second nickel layer on top of the original structure. Since this new Ni/Al/Ni structure has proven to be stable during the 1000-hour damp heat test it has been incorporated into the baseline and is now used also for gridded mini-modules.

6.6 Module degradation

When cells are monolithically integrated into modules, functional parts are added that have a potential impact on long-term stability. A commonly used interconnect structure is shown schematically in a cross section view in Figure 42.

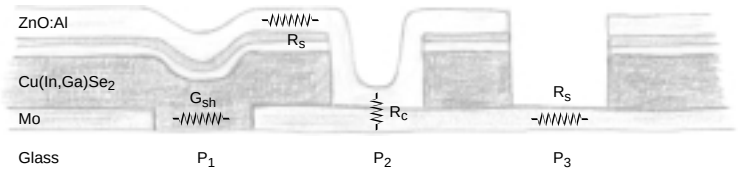

Figure 42. Interconnect structure for CIGS modules.

Here, potential stability issues are indicated by resistor symbols. The degradation of the shunt path through the CIGS absorber in the back contact scribe (P_1), and the

ZnO:Al/Mo contact in the interconnect via (P_2) during accelerated lifetime testing is investigated in Paper III. Furthermore, the ZnO:Al front contact degradation as well as corrosion of the exposed molybdenum back contact in the isolation scribe (P_3) are evaluated. These mechanisms are addressed in more detail also in the following sections.

With input from previous experimental studies on degradation of cells and modules, the spreadsheet model previously described (see section 4.2) has been used in Paper VIII to calculate the evolution of power losses during accelerated ageing of two different non-encapsulated mini-modules, one conventional and one gridded, and a baseline reference cell. Also here, the reference level is an ideal cell of 15% active area efficiency exhibiting 30 mA/cm^2 at its maximum power point. The purpose of the power loss calculation is to find those functional module components that are of particular importance from a stability point of view, and to demonstrate the relative difference in power loss between these components for different devices. Results from the calculation are given in Figure 43.

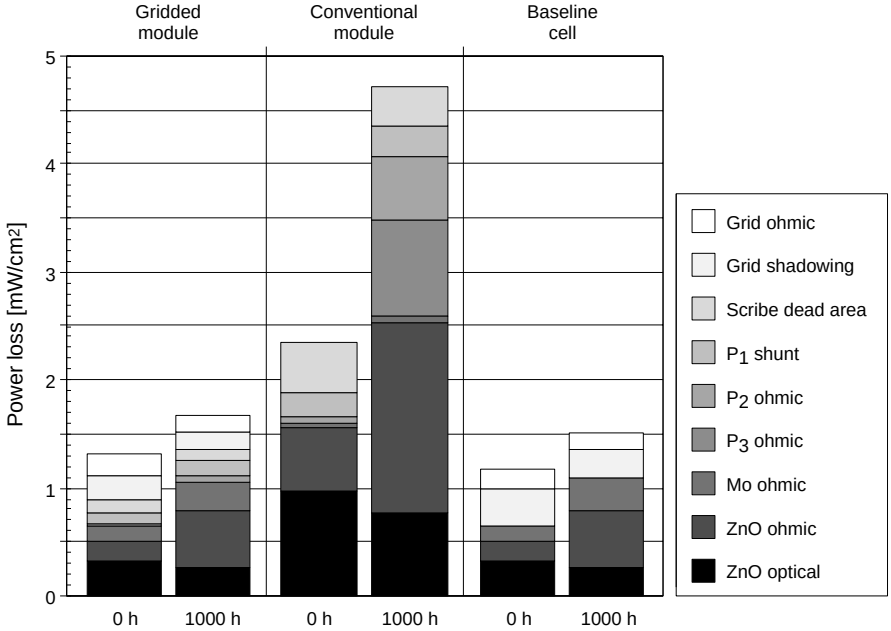

Figure 43. Calculated power losses of a conventional and a gridded module, compared to that of a reference baseline cell, before and after 1000 hours of damp heat exposure. All devices are non-encapsulated.

The baseline cell experiences losses additional to the reference level that are approximately 1.2 mW/cm^2 in the as-grown state and that increases to 1.5 mW/cm^2 after extended damp heat exposure. For the conventional module, the losses are 2.3 mW/cm^2, as grown, and 4.7 mW/cm^2 aged. Relative to the baseline cell, the losses of the conventional module are significantly higher. This difference appears primarily in the front contact. The gridded module experience losses similar to those of the baseline cell, both for as-grown and aged devices. The reason for this

is that the design of this module was chosen similar to that of the reference cell (see Papers IV and VII for further discussion on this module design). The degradation mechanisms listed in Figure 43 are addressed in the following sections.

6.6.1 Front contact issues

Other studies have concluded that apart from corrosion of the molybdenum back contact in the cell isolation scribe (see section 6.6.4), degradation of the electrical properties of the ZnO:Al front contact is the primary cause of performance loss for modules [89]. This is, however, not in line with the experience gained in the present work. In Paper I, the evolution of the optical and electrical properties of the front contact during accelerated ageing are investigated, and it is concluded that the sheet resistance increase of the ZnO:Al during a 1000 hour extended damp heat test is too low to have a major impact on cell performance. A similar conclusion is made for modules in Paper III.

The resistivity of baseline ZnO:Al is generally observed to increase linearly with time during accelerated ageing. After the standard 1000 hours in damp heat conditions, the sheet resistance is in the order of two to three times that of the as-grown films, and, as can be seen in Figure 44, is still on a linear increase after nearly 3000 hours. Unlike device performance, the window degradation appears to not saturate. In previous studies, it has been shown that the as-grown performance of the ZnO:Al front contact is dependent on the thickness of the CdS used [58]. In addition to that study, it is investigated in Paper I whether the CdS also has an influence on the long-term stability of the ZnO:Al. In this context, the influence of sodium was also addressed. From this study it can be concluded that the ZnO:Al degradation is enhanced by the presence of CdS and further enhanced with increasing CdS thickness. But since the CdS-free samples also exhibit degradation, although not at the same rate, the CdS alone cannot be the cause. Instability is also seen for the window deposited on sodium free substrates, indicating that the degradation is not uniquely a sodium related issue.

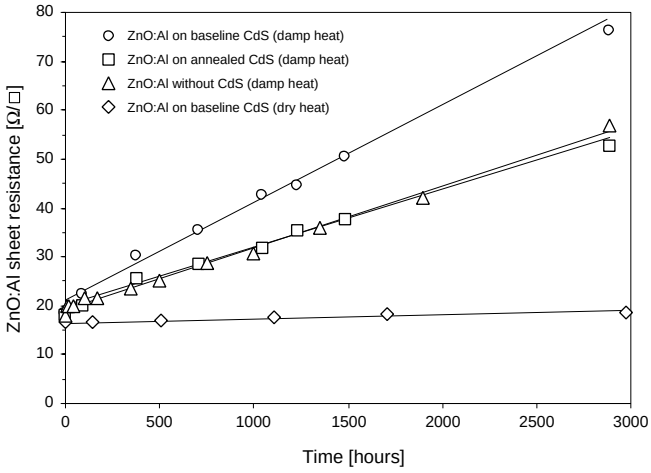

Figure 44. Accelerated ageing tests of various ZnO:Al/CdS structures, comparing the stability of ZnO:Al grown on no, annealed, and baseline CdS on glass substrates.

A set of experiments where the CdS was annealed at 300 °C for 3 hours in argon atmosphere prior to ZnO:Al deposition, shows that the stability is improved. As seen in Figure 44, the degradation rate of annealed samples with CdS is similar to that of samples without CdS. It has been shown that CdS in damp heat conditions absorb additional water, and that the impurities in the CdS are strongly modified [90]. If this has an impact on the stability of the ZnO:Al remains to be investigated.

By studying absorption data, calculated from transmission and reflection measurements of windows grown on soda-lime glass, it is clear that extended damp heat exposure affects the optical properties of the ZnO:Al (Paper I). A comparison of the calculated current loss for windows with different CdS layer thickness in two complementary parts of the spectrum, i.e. at photon energies above and below the bandgap of CdS, shows that the current loss in the CdS itself is not affected by ageing, but that the presence of CdS has an influence on the ZnO:Al absorption. ZnO:Al front contacts without the CdS buffer are not only the most stable, but also exhibit considerably less current loss. Unfortunately CdS-free devices do not yet have the junction qualities of conventional devices, although several recent studies on alternative buffers show promising results [91]. Good results have also been obtained for CIGS devices without intermediate buffer layers [92].

In Paper II, the effect of the high-resistive ZnO buffer layer on the long-term stability of CIGS cells is investigated. Figure 45 shows the relative stability of cells with and without the ZnO buffer layer for two different cells exposed to damp heat conditions. From this study it appears that cells without the ZnO buffer are more sensitive than baseline devices to hot and humid environments.

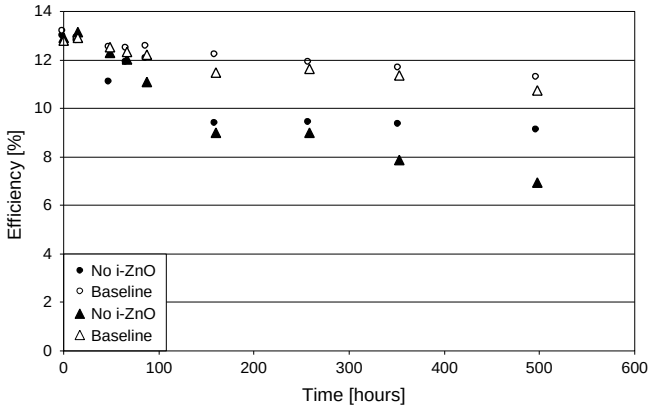

Figure 45. Accelerated ageing in damp heat conditions of CIGS devices with and without the high-resistive ZnO buffer layers.

6.6.2 Cell definition scribe (P_1)

The issue of interconnect degradation is addressed in Paper III by comparing the long-term stability of cells and mini-modules fabricated within the frames of the baseline (see section 3.2). Although the CIGS absorber as well as the CdS buffer and the ZnO:Al/ZnO front contact were similar for all devices, it was observed that modules experienced a more pronounced degradation in open circuit voltage than cells. From the previously discussed explanations to voltage degradation there is

no reason to expect a different behavior for cells and modules. Looking at the monolithic series integration of cells into modules, the shunting of current through the cell definition scribe (P_1, see Figure 42) is the only functional part of the interconnect that may have an impact on the open circuit voltage degradation. An increasing shunt conductance through P_1 would theoretically cause a voltage loss, but simulations carried out in Paper III show that if the P_1 shunt was large enough to explain the observed difference in open circuit voltage between modules and cells, it would also result in a fill factor loss much more severe than the actually observed. Moreover, results from measurements of the shunt conductance give no clear trend of increase with damp heat exposure.

6.6.3 Interconnect via (P_2)

Degradation of the contact properties of the P_2 interconnect via has been discussed in Paper III, where it is argued to be one of the primary causes of module degradation. Suggested explanations to this phenomenon are that a resistive oxide layer is formed between the ZnO:Al and the molybdenum, or that the ZnO:Al is depleted of free carriers in a thin layer close to the interface.

6.6.4 Back contact corrosion (P_3)

Corrosion of the molybdenum back contact is a degradation mechanism that is proven to be detrimental to module performance. This was first published in Paper I, and later investigated in more detail in Paper III. Both for encapsulated and bare devices, the effect occurs in the cell isolation scribes when the devices are exposed to humidity. After extended damp heat exposure, the corrosion results in a major fill factor loss. This effect has been confirmed by several research groups [89, 38].

Molybdenum oxidizes rapidly in damp heat conditions and forms the non-conductive, milky MoO_3. Figure 46 shows photographs of the evolution of corrosion on a 0.2 cm^2 bare molybdenum sample during damp heat exposure. The corrosion starts in point defects, which for modules may be caused by scratches from the scribing process or by sandblasting during edge preparation. From the original defects, the corrosion tends to grow laterally with time and form clusters of larger corroded areas. As the affected areas develop further, the sheet resistance increases exponentially.

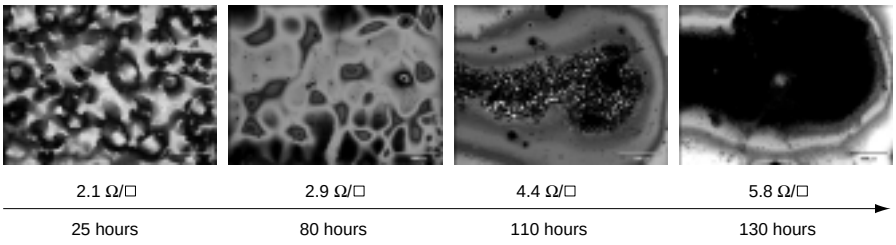

Figure 46. Corrosion of bare molybdenum. The photographs of a 0.2 cm^2 bare molybdenum sample are correlated to sheet resistance measurements during damp heat exposure.

Although the corrosion has a rather rapid evolution, it will last long before any effect is seen on the fill factor of devices. After 500 hours of damp heat exposure the sheet resistance of the molybdenum in the P_3 cell isolation scribe has increased by about a factor of 100. However, since the scribe is very narrow, only about

50 μm, this has little impact on module performance. Not until the back contact has corroded severely, which for non-encapsulated devices may last longer than 500 hours, the performance is drastically reduced. In Paper III it is shown that the sheet resistance of molybdenum in the cell isolation scribe would have to increase by three orders of magnitude in order to cause a fill factor loss of 10% (relative). In practice, no effect will be seen on module performance until the molybdenum in the scribe has oxidized completely and the interconnect is broken. For the power loss calculation above (see section 6.4), a lower P_3 degradation rate than has been observed experimentally is assumed.

6.7 Encapsulation

An effort on evaluating different encapsulants (see section 3.3) has been initiated. Bare baseline molybdenum films grown on 5×5 cm^2 soda-lime glass substrates were laminated with a cover glass, using EVA, silicone, or thermoplastic films. Initial stability tests with the different encapsulants indicate that neither EVA, which is dominating the photovoltaics industry today, nor the other tested materials are satisfying. Figure 47 shows the samples after 1000 hours in damp heat conditions. The EVA (left) and the silicone (middle) appear to provide the best protection, while the thermoplastic (right) has delaminated completely.

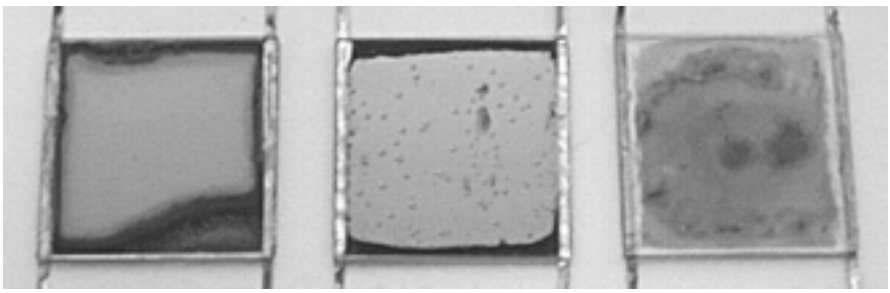

Figure 47. Encapsulated molybdenum films after 1000 hours of damp heat exposure. The films are laminated with a cover glass using three different encapsulants (from left to right): EVA, silicone, and thermoplastics.

7 Towards sustainable photovoltaics

An interesting question from a materials point of view is why, out of an almost infinite number of theoretically possible compounds and a very large number of experimentally tested materials, only a handful of materials have emerged as good solar cell absorber layers. One reason is certainly that many chemical, physical and practical boundary conditions have to be fulfilled simultaneously. Nevertheless, the search for new materials has mainly been carried out on an empirical basis, and no good theoretical guidelines exist for predicting which material that will have the exact properties needed for this purpose [93]. Looking at the long history of research of thin film materials it appears very difficult to find an entirely new material among the inorganic semiconductors. This may be different if new classes of materials are considered, or if new photovoltaic effects are discovered. According to [93], requirements for the ideal solar cell material include a bandgap between 1.1 and 1.7 eV, a direct band structure, and high photovoltaic conversion efficiency. These conditions are all fulfilled by several of today's thin film candidates, including CIGS, CdTe, and eventually also amorphous silicon in multi-junction structures. However, several issues can be identified as critical targeted areas of research and development to accelerate the progress towards large-scale implementation of photovoltaics. These issues include

- easy, reproducible deposition techniques, suitable for large area production;
- proven long-term stability;
- using abundant, available, non-toxic materials and environmentally benign fabrication processes.

Whether the CIGS technology fulfils these issues is discussed in the following sections.

7.1 Manufacturability

With multiple groups reporting efficiencies above 15% for small-area CIGS cells, the challenge now facing the photovoltaics industry is to scale up the technology with maintained performance, i.e. to bring the efficiencies of large-area industrial modules closer to those of small laboratory cells. For large-scale module fabrication, the critical issues are high material quality over large areas, throughput, reproducibility, and process yield.

Up-scaling of the deposition processes for the zinc oxide front contact and the molybdenum back contact is rather straightforward. These layers are fabricated by sputtering, which is a well established large-area coating technique, widely applied in the food packaging industry as well as for coating of windowpanes in the glass industry. For the ZnO:Al front contact, the optimum film properties depend on the module design, i.e. the cell width, and the absorber composition. RF sputtering from ceramic ZnO targets normally yields the best film properties, but deposition rates and the perspectives for large area up-scaling are limited. DC sputtering from ceramic ZnO targets gives higher deposition rates and easy up-scaling, and is also favorable from a materials cost point of view. Similar arguments apply for the molybdenum back contact deposition.

The true challenge lies in the up-scaling of the CIGS fabrication step. A potential manufacturer should of course be encouraged by the wide variety of manufacturing techniques for CIGS films. These include co-evaporation, seleniza-

tion of sputtered or evaporated stacked metal layers, and metal organic chemical vapor deposition, as well as non-vacuum techniques such as screen-printing and electro-deposition. Generally, the non-vacuum techniques have yielded relatively poor efficiencies. Siemens Solar Industries, so far the only manufacturer of commercial CIGS-based modules, have chosen to work with the selenization process, in which the metal layers are sequentially sputtered onto the substrate at room temperature and thereafter annealed in selenium atmosphere at a temperature of about 550 °C. The second major player, Würth Solar, is presently close to commercialize their technology, which is based on co-evaporation of the four elements from linear sources onto a substrate heated to about 550 °C. This might be a technically more complicated task to accomplish, but have the advantage of rendering higher quality material, and thus potentially better performing modules. Which of these two approaches that is the most cost-effective is yet to be proven.

Substantial knowledge of manufacturability can be gained from laboratory small-scale experiments with cells and mini-modules. As has been discussed previously (see section 4), the issues in design of mini-modules resemble much those of full size production modules. This includes constraints on the properties of the front contact, which can be eased in a number of ways as has been discussed previously, for example by increasing the gallium content in the absorber or using gridded modules. Other issues that need to and can be addressed on a laboratory scale include the necessity of sodium diffusion from the soda-lime glass through the molybdenum back contact and a corresponding optimization of the molybdenum thickness. Regarding manufacturability of the CIGS absorber itself, independently of growth process, some of the more important research issues are listed in [94] and include

– a better understanding of the defect chemistry and intrinsic doping mechanism in $Cu(In,Ga)(S,Se)_2$ films to get easy control over free-carrier concentration and doping profiles in the films;
– a comprehensive understanding of the surface chemistry and structure of the $Cu(In,Ga)(S,Se)_2$ absorber aiming at constructing a junction interface with minimum recombination and possibly containing an inversion layer in combination with a window layer that is easy to integrate into the process sequence;
– to produce wide-bandgap alloys of $Cu(In,Ga)(S,Se)_2$ with bandgaps between 1.4 and 1.5 eV to enhance open circuit voltage while maintaining performance;
– to reduce the $Cu(In,Ga)(S,Se)_2$ absorber thickness to less than 1 μm, while maintaining performance;
– to monitor in situ for diagnostics and quality control for intellectual processing of the different layers.

7.2 Environmental issues

Since photovoltaics does not generate any emissions during operation, the environmental impacts are mainly associated with emissions related to production of modules and their disposal at the end of their service life. In addition, there are concerns about material constraints as new technologies such as CIGS and CdTe enter large-scale production.

7.2.1 Toxicity

One of the primary considerations about the environmental impact of CIGS thin film modules concerns cadmium, which is considered the most toxic among the elements used in this kind of solar cells. Cadmium is a lung carcinogen and is known to have long-term effects on the kidney and bone. However, cadmium like most of the elements used in photovoltaic modules is bound in compounds that are not easily soluble. Therefore, the long-term health risks with disposed modules are likely to be very low. The acute health effects from inhaling cadmium include pneumonitis, pulmonary edema, and death [95]. In large-scale plants, a release of toxic materials is likely to occur only as a result of accidents or abnormal plant operations and therefore poses only a small risk to public health.

In a report on several studies on the toxicity of CdTe, CIS and CGS [95], it is concluded that CdTe is the most toxic of the three compounds, followed by CIS and CGS. Furthermore, cadmium and tellurium are said to be considerably more toxic than gallium or indium, and indium is considered more toxic than gallium. Although all three compounds are considered to be relatively insoluble in water, CdTe was found to be more soluble than CIS or CGS, particularly in conditions resembling lung fluids. Both indium and gallium were found to shorten the life spans of rats and mice. More details on these studies are given in [95].

CIGS modules have undergone extensive testing for fire and leaching [96], as well as potential mechanisms for recycling and disposal [97]. The results are generally positive from a toxicity point of view, and indicate a minimal impact on the environment. In [96] for example, it is concluded that only small amounts of critical elements, far smaller than the limits for exposure suggested by government and independent agencies, will be mobilized if disposed CIGS modules were to be used as landfill or in case of an accident. The over-all content of critical substances in a CIGS module are said to be low compared to average waste.

It is generally understood that all chemicals are toxic at some dose. The most common subjects for toxicology studies on semiconductor metals so far are human cells and small mammals such as rats and mice, but aquatic organisms may be at a much higher risk due to uptake of low-molecular substances through skin and gills. Furthermore, toxic substances bound to particulate matter, are easily taken up as food by bottom-dwelling animals that constitute an early stage in the food chain.

With the exception of cadmium, surprisingly little is known about the impact of semiconductor metals on the stability of the ecosystem and the indirect long-term effects on humans. A brief literature survey has resulted in only very few publications on bioaccumulation of semiconductor metals and the effects on aquatic organisms. In [98] for example, it is reported that indium in the form of indium chloride has a significant negative impact on the development of fish embryos. Furthermore, it is shown in [99] that selenium, which, in low doses, is an essential micronutrient for many organisms, easily accumulates in the food chain and can reach toxic levels in fish although no impact can be detected on the prey species. Considering that human is at the top of the food chain, effects like this might be at least as important as the direct toxic effects in a long-term perspective. The few so far determined limits for environmental exposure of semiconductor metals are not based on scientific studies but on scarce empirical data [100].

Before bringing any new technology, photovoltaic or other, into mass production, it is important to fully investigate its impact on environment, both short-term

and in a broader perspective. This will require joint efforts by researchers from within several scientific disciplines, as well as the cooperation from manufacturers and surveillance by governmental and independent agencies.

7.2.2 Recycling

There are, to date, no established recycling of disposed photovoltaic modules. The reason for this is most likely that modules generally have a long service lifetime, and that the quantity of disposed modules so far is small enough to not be considered a problem. However, as photovoltaics is steadily increasing its share of global power production this situation might change over the next two or three decades, and developing sustainable recycling schemes is becoming urgent. To illustrate this need, a parallel can be drawn to nickel-cadmium batteries that contain considerably more cadmium per watt than for example CIGS solar cells. Batteries of nickel-cadmium type have been on the market for some 20 years, and there are well-established recycling programs. Nevertheless, a recent American study conclude that only about 10% of the small consumer nickel-cadmium batteries were recycled in the USA in year 2000 [97]. Compared to batteries, recycling of solar panels is even more complicated. This is because of the decades-long intervals between installing and discarding modules, their low concentration of valuable materials, and their geographical dispersion. In addition, metals like cadmium and lead, although their concentration in a solar panel is minuscule, may cause a hazardous waste classification, with all the associated cost implications. The lack of significant quantities of any key material makes it unlikely that the recovery of materials from spent modules is economically warranted with today's metal prices. However, if prices on the minor metals involved will rise due to increased demand and low availability (see section 7.2.3), this picture might change drastically.

7.2.3 Material constraints

All photovoltaic systems rely on metals to a large extent, both in semiconductor compounds and as its contacts, as well as for module frames, connectors, and supporting structures. As photovoltaics is increasing its small but steadily growing fraction of the global power production, the demand for metals will increase. In particular, mass production of the emerging thin film technologies would lead to accelerated mining of the elements cadmium, tellurium, indium, gallium, selenium, germanium and ruthenium, which could increase sulphur dioxide emissions and metal leakage from waste dumps, and cause large-scale land transformations [101].

For CIGS solar cells, the metals indium, gallium, selenium, and cadmium are of particular interest since they are considered rare or geochemically scarce compared to base metals such as copper, zinc and aluminum. Due to low grades in combination with relatively low prices, these elements are recovered today as by-products. Selenium is a by-product of copper refining while indium and cadmium are mainly a by-products from zinc recovery. Also gallium is somewhat concentrated in zinc ore, but is mainly recovered from bauxite. The availability of these minor metals depends on mining primarily driven by demand for base metals, on recovery from mined ore and on recycling of secondary materials. According to a recent study on the prospect for increased mining of these minor metals [101], their annual output is likely to continue to be heavily dependent on the long-term development and short-term fluctuations of the market situation of the major metals. However, assuming a potential willingness to pay for the minor metals, it is

not impossible that demand for these metals could become an additional driving force for increased mining [101]. Substantially raised prices could also lead to new discoveries and draw attention to resources that have previously been overlooked.

The issue of material constraints can also be addressed in the manufacturing process by lowering the required amounts of metals. This can be achieved by partly replacing specific elements. In the case of CIGS, gallium is used to substitute indium to some extent, which has a number of other benefits as well. However, at some level there will be a trade-off between substitution and device performance. This is further discussed in section 4.4. In addition, much of the current CIGS research include ways of using less materials to produce the same output, either through higher materials utilization, thinner films, or higher module efficiencies. However, the metal demand from solar cell production will not be significant for many years, so the options for reducing materials used might not be economically warranted until metal prices have risen substantially and module production costs come closer to long-term goals.

7.3 Long-term stability

Proven long-term stability is a fundamental requirement for any new photovoltaic technology to be a commercial success. Field tests of CIGS-based devices have indicated stable performance over several years, but as discussed in the previous chapters, failures are frequently observed in accelerated lifetime tests. It might be necessary to revise the standard accelerated test procedures to be more relevant for thin film technologies [81], but a fact is that today's thin film solar cells are more sensitive to humidity than the conventional crystalline silicon technology. One possible solution to the stability problem is to improve the encapsulation technology, but the fact that little is known about the complex solid state chemistry involved raises concerns about undesired chemical reactions in the long run, also for perfectly encapsulated devices. Enhanced understanding of the mechanisms involved in device degradation is needed as the CIGS technology emerges towards large-scale production, and this has motivated several research institutions, including the Ångström Solar Center, to study ageing of CIGS devices.

7.3.1 Improved encapsulation technology

Results from accelerated ageing of encapsulated CIGS modules (see Figure 50 below) indicate that EVA, which is the standard encapsulant for crystalline silicon modules, provides insufficient protection from the environment for CIGS modules. This has been confirmed by other research institutions as well [89]. As discussed in section 6.4, humidity penetrating through the encapsulation causes performance loss due to increasing defect density in the bulk of the absorber, degradation of the electrical properties of the front contact, and corrosion of the back contact. It has been reported that CIGS modules have successfully passed the standard accelerated lifetime tests with EVA as encapsulant, but in these cases, a modified encapsulation technology was used [79, 32]. However, any details on these improved encapsulations have so far not been presented. Ideas on improved encapsulation include edge sealing by metal wires or glass bonding, as well as alternative encapsulants such as silicones or thermoplastics. However, it is left to be proven whether the encapsulation by either of these techniques is economically viable.

7.3.2 Design for long-term performance

In Paper VIII, the stability problem is approached from a slightly different angle. Here it has been studied to what extent the degradation of a CIGS module can be compensated for by choosing a smart design of the module. Rather than optimizing the initial efficiency, the module has been designed for good long-term performance. This, of course, involves a number of assumptions concerning degradation rates of various functional components of the module, assumptions that are valid only for given fabrication processes. The approach is to minimize the impact from those parts of the module that can be expected to contribute significantly to device degradation. Special attention is paid to the degradation of the interconnects and the transparent front contact.

As discussed above, degradation of the ZnO:Al front contact typically appears as an increasing sheet resistance. For the conventional module, the effect of this on performance may be reduced by narrowing down the segment width or by modifying the ZnO:Al process in order to obtain films with higher conductance. For the gridded module, the ohmic losses in the ZnO:Al can be controlled by varying the spacing between the grid fingers. To a first approximation, the spacing can be chosen independent of segment with. Thus, the gridded design is preferable from a long-term performance point of view. Optimizing the interconnects of the conventional module is a trade-off between area loss, ohmic losses and shunting. Shunting through the CIGS in the P_1 cell definition scribe is proportional to the cell voltage and inversely proportional to the width of the scribe and the resistivity of the CIGS. In order to compensate for the expected increasing shunting losses, as the resistivity decreases with time, the width of the P_1 scribe should be chosen larger than what is optimal for an as-grown device. This will however impact the active area. At the same time, the expected voltage degradation is actually beneficial from a shunting point of view. Assuming that the gridded module has wider segments than the conventional, this design is less sensitive to P_1 shunting since the shunted current is smaller relative to the generated current for each cell. To compensate for the expected increasing contact resistance in the P_2 interconnect via, the scribe can be widened. Gridded modules have a metal-to-metal P_2 contact that is assumed to be more stable.

The benefit of designing modules for long-term performance is illustrated in Figure 48. Here, the efficiencies are calculated and plotted for as-grown and aged conventional and gridded modules. These are compared to the efficiencies of modules with improved designs. As can be seen, the improved modules have lower initial efficiencies but are more durable. For the conventional module in this example, enhanced long-term performance is achieved by increasing the widths of P_1 and P_2, and reducing the segment width. The gridded module has a thinner and therefore more transparent ZnO:Al front contact, and the spacing between the grid fingers is reduced. It is assumed that the corrosion of molybdenum in P_3 is suppressed.

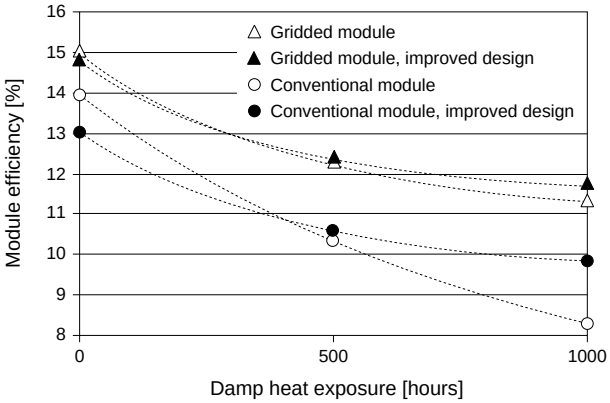

Figure 48. Calculated evolution of the efficiencies of non-encapsulated gridded and conventional modules with standard and improved design during accelerated ageing. The calculations are based on experimentally obtained values of degradation of module components, and are presented in more detail in Paper VIII.

7.3.3 Smart patterning

The choice of patterning technology is important, in particular for the P_3 cell isolation scribe. Mechanical scribing of P_3 often cause severe scratching of the molybdenum back contact, which is found to accelerate the corrosion process. Ideally, from an active area point of view, P_3 should be as thin as possible. This is also beneficial for long-term stability of the device since the effect of back contact corrosion becomes lesser. For the conventional module it is possible to further delay both P_2 and P_3 degradation by choosing smart patterning technologies. A novel interconnect structure with better long-term stability properties is proposed in Paper VIII. The structure of this interconnect is shown schematically in Figure 49. Here, the CIGS is not removed from the P_2 interconnect via as with mechanical scribing. Instead, it is locally transformed into a conductive state by using a laser. Also P_3 can be patterned by methods alternative to mechanical scribing. By using photolithography it is possible to remove only the conductive ZnO:Al, leaving the CIGS to protect the molybdenum back contact from corrosion. However, photolithography might not be the first choice from a manufacturing point of view. Another option is to remove the front contact by laser. A fully laser fabricated interconnect would be advantageous from a processing point of view.

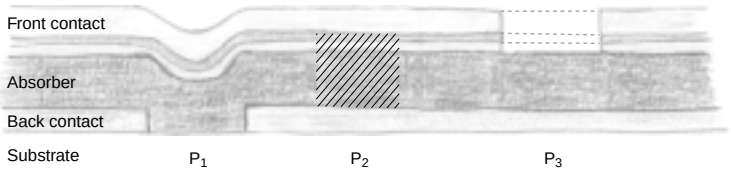

Figure 49. A novel interconnect structure, designed for enhanced long-term performance.

A 5×5 cm^2 mini-module based on the novel interconnect structure has been fabricated and exposed to damp heat conditions. As shown in Figure 50, the initial efficiency of the non-encapsulated module was relatively low, probably due to a

poor P_2 contact that was performed by a not so well developed laser process. However, compared to a commercially available Siemens ST10 CIGS module, the non-laminated mini-module is much more performant after 1000 hours of damp heat exposure. This is just a first experimental result with the novel interconnect structure, but it indicates that the stability issue can be addressed without costly modifications of the standard EVA technology.

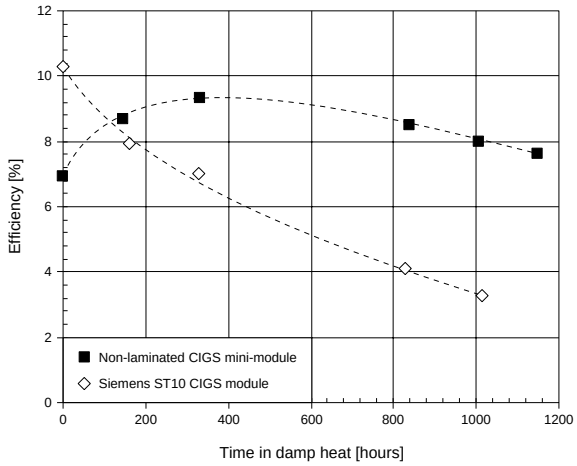

Figure 50. Results from damp heat testing of a CIGS module based on the novel interconnect structure, compared to a commercially available Siemens ST10 module.

Acknowledgements

Looking back at nearly six years of work, it is of course tempting to list all those who have had an impact during this period, but I will just mention a few that have been truly outstanding.

During the first year as a PhD student, I drifted a bit aimlessly in the squalls between various lab chores until this funny looking fellow *John Kessler* appeared and set the course. I sometimes think that this work would not have been accomplished without the encouragement from John, always available for discussion and ready to scrutinize any method or result to perfection. I am also very grateful to *Lars Stolt* for having introduced me to this exciting field of research, and for providing excellent guidance from time to time. I have often been both amazed and encouraged by Lars' intellectual capacity and ability to navigate through turbid waters. Another pleasant chap is *Olle Lundberg*, whom in many different ways has embellished my days at work and helped me sorting out the essentials in life. I am greatly thankful to *Jonas Malmström* for his invaluable contribution, scientifically and in other respects, to making the last year particularly interesting.

Of course, many other colleagues, as well as family and friends, have made deep impressions in their own personal ways during the years, and this has probably been much more important than they realize. I hope I will be able to thank you all in person in due time.

On a cold winter day,

Johan Wennerberg

References

[1] E. Lorenzo, *Solar Electricity, Engineering of Photovoltaic Systems*, PROGENSA, (1994)

[2] *World Energy Outlook 2000*, International Energy Agency (2000)

[3] D. Munro and E. Rudkin, *Trends in PV Power Applications in Selected IEA Countries Between 1992 and 1997*, Report IEA PVPS 1-06 (1998)

[4] J. Goldemberg, ed., *World Energy Assessment: Energy and the challenge of sustainability*, United Nations Development Programme (UNDP) (2000)

[5] O. Beckman, *Ångström – Father and Son*, Acta Universitatis Upsaliensis **C 60** (1997)

[6] *ASTM E 490 Standard Solar Constant and Air Mass Zero Solar Spectral Irradiance Tables*, **27** American Society for Testing and Materials (1973)

[7] *Solar Simulation*, Oriel Corporation (1993)

[8] Hermann Scheer, *Sonnen Strategie – Politik Ohne Alternative*, R. Piper GmbH & Co. KG, München (1993)

[9] P. E. Glaser, and others, *Solar Power Satellites: A Space Energy System for Earth*, John Wiley and Sons (1997)

[10] D. M. Chapin, C. S. Fuller, and G. L. Pearson, *A New Silicon p-n Junction Photocell for Converting Solar Radiation into Electrical Power*, J. Appl. Phys. **25** (1954) 676–677

[11] W. Hoffman, *PV Solar Electricity: One Among the New Millennium Industries*, to be published in proceedings 17th European Photovoltaic Solar Energy Conference (2001)

[12] B. van Campen, D. Guidi, and G. Best, *Solar photovoltaics for sustainable agriculture and rural development*, FAO (2000)

[13] C. E. Witt, R. L. Mitchell, H. P. Thomas, and M. Sumko-Davies, *Terrestrial Photovoltaic Technologies Update*, Renewable Energy **23** (2001) 349–353

[14] H. von Campe, G. H. Hewig, W. Hoffmann, H. Huschka, B. Schurich, and J. Wörner, *Detailed Analysis of a Pilot Line Production Process for Cu_2S/CdS Thin Film Solar Cells and the Layout of a Production Line*, in proceedings 6th European Photovoltaic Solar Energy Conference (1985) 778–786

[15] L. D. Partain, P. S. McLeod, J. A. Duisman, T. M. Peterson, R. E. Weiss, and C. S. Dean, *Degradation of Cu_x/CdS in Hot, Moist Air: Experiment and Theory*, in proceedings 16th IEEE Photovoltaic Specialists Conference (1982) 883–887

[16] D. W. Cunningham, K. Davies, L. Grammond, J. Healy, E. Mopas, N. O'Connor, M. Rubcich, M. Sadeghi, D. Skinner, and T. Trumbly, *BP Solarex – Large Area Apollo® Thin Film Module Development*, in proceedings 16th European Photovoltaic Solar Energy Conference (2000) 281–285

[17] R. D. Wieting, *CIS Product Introduction: Progress and Challenges*, AIP Conf. Proc. **462** (1999) 3–8

[18] D. E. Carlson and C. R. Wronski, *Amorphous Silicon Solar Cell*, Appl. Phys. Lett. **28** (1976) 671–673

[19] D. L. Staebler and C. R. Wronski, *Reversible Conductivity Changes in Discharge-Produced Amorphous Si*, Appl. Phys. Lett. **31** (1977) 292–294

[20] A. Shah, P. Torres, R. Tscharner, N. Wyrsch, and H. Keppner, *Photovoltaic Technology: The Case for Thin-Film Solar Cells*, Science **285** (1999) 692–698

[21] K. D. Dobson, I. Visoly-Fisher, G. Hodes, and D. Cahen, *Stability of CdTe/CdS Thin-Film Solar Cells*, Solar Energy Materials & Solar Cells **62** (2000) 295–325

[22] P. Rappaport, *The Photovoltaic Effect and its Utilization*, RCA Review **20** (1959) 373–397

[23] D. Bonnet and H. Rabenhorst, *New Results on the Development of a Thin Film p-CdTe-n-CdS Heterojunction Solar Cell*, in proceedings 9th IEEE Photovoltaics Specialists Conference (1972) 129–131

[24] H. Uda, H. Matsumoto, Y. Komatsu, A. Nakano, and S. Ikegami, *All Screen Printed CdS/CdTe Solar Cell*, in proceedings 16th IEEE Photovoltaic Specialists Conference (1982) 801–804

[25] J. Skarp, Y. Koskinen, S. Lindfors, A. Rautiainen, and T. Suntola, *Development and Evaluation of CdS/CdTe Thin Film PV Cells*, in proceedings 10th European Photovoltaic Solar Energy Conference (1991) 567–569

[26] R. W. Birkmire, *Compound Polycrystalline Solar Cells: Recent Progress and Y2K Perspective*, Solar Energy Materials & Solar Cells **65** (2001) 17–28

[27] S. J. Fonash, *Solar Cell Device Physics*, Academic Press Inc. (1981)

[28] H. J. Möller, *Semiconductors for Solar Cells*, Artech House Inc. (1993)

[29] M. A. Contreras, B. Egaas, K. Ramanathan, J. Hiltner, A. Swartzlander, F. Hasoon, and R. Noufi, *Progress Toward 20% Efficiency in Cu(In,Ga)Se_2 Polycrystalline Thin-Film Solar Cells*, Progress in Photovoltaics: Research and Applications **7** (1999) 311–316

[30] J. Kessler, M. Bodegård, J. Hedström, and L. Stolt, *New World Record Cu(In,Ga)Se_2-Based Mini-Module: 16.6%*, in proceedings 16th European Photovoltaic Solar Energy Conference (2000) 2057–2060

[31] H. S. Ullal, K. Zweibel and B. G. von Roedern, *Current Status of Polycrystalline Thin-Film Technologies*, in proceedings 26th IEEE Photovoltaic Specialists Conference (1997) 301–305

[32] F. Karg, H. Calwer, J. Rimmasch, V. Probst, W. Riedl, W. Stetter, H. Vogt, and M. Lampert, *Development of Stable Thin Film Solar Modules Based on $CuInSe_2$*, Inst. Phys. Conf. **152** (1998) 909–913

[33] R. M. Swanson, *The Promise of Concentrators*, Progress in Photovoltaics: Research and Applications **8** (2000) 93–111

[34] H. Hahn, G. Frank, W. Klingler, A. Meyer, and G. Störger, *Über Einige Ternäre Chalkogenide mit Chalkopyritstruktur*, Z. anorg. u. allg. Chemie **271** (1953) 153–170

[35] S. Wagner, J. L. Shay, P. Migliorato, and H. M. Kasper, *$CuInSe_2$/CdS Heterojunction Photovoltaic Detectors*, Applied Physics Letters **25** (1974) 434–435

[36] R. A. Mickelsen and W. S. Chen, *Polycrystalline Thin-Film $CuInSe_2$ Solar Cells*, in proceedings 16th IEEE Photovoltaic Specialists Conference (1982) 781–785

[37] K. C. Mitchell, J. Ermer, and D. Pier, *Single and Tandem Junction $CuInSe_2$ Cell and Module Technology*, in proceedings 20th IEEE Photovoltaic Specialists Conference (1988) 1384–1389

[38] F. Karg, *Development and Manufacturing of CIS Thin Film Solar Modules*, Solar Energy Materials & Solar Cells **66** (2001) 645–653

[39] M. Powalla and B. Dimmler, *First Results of the CIGS Solar Module Pilot Production*, to be published in proceedings 17th European Photovoltaic Solar Energy Conference (2001)

[40] K. Kushiya, M. Tachiyuki, Y. Nagoya, A. Fujimaki, B. Sang, D. Okumura, M. Satoh, and O. Yamase, *Progress in Large-Area Cu(InGa)Se_2-Based Thin-Film Modules with a Zn(O,S,OH)$_x$ Buffer Layer*, Solar Energy Materials & Solar Cells **67** (2001) 11–20

[41] J. Kessler, M. Bodegård, J. Hedström, and L. Stolt, *Baseline Cu(In,Ga)Se_2 Device Production: Control and Statistical Significance*, Solar Energy Materials & Solar Cells **67** (2001) 67–76.

[42] J. Ermer, R. Gay, D. Pier, and D. Tarrant, *Challenges and Progress in the Scale up of $CuInSe_2$ Thin Film Photovoltaic Technology*, Journal of Vacuum Science Technology A **11** (1993) 1888

[43] S. Raud, J. S. Chen, and M-A. Nicolet, *Influence of Oxygen on Diffusion in the Cu/Mo/Au System*, Appl. Phys. A **52** (1991) 151–153

[44] K. Granath, *The Influence of Na on the Growth of Cu(In,Ga)Se_2 Layers for Thin Film Solar Cells*, Thesis, Acta Universitatis Upsaliensis, Uppsala (1999)

[45] J. Hedström, H. Ohlsén, M. Bodegård, A. Kylner, L. Stolt, D. Hariskos, M. Ruckh, and H. W. Schock, *ZnO/CdS/Cu(In,Ga)Se_2 Thin Film Solar Cells with Improved Performance*, in proceedings 23rd IEEE Photovoltaic Specialists Conference (1993) 364–371

[46] M. Bodegård, L. Stolt, and J. Hedström, *The Influence of Sodium on the Grain Structure of $CuInSe_2$ Films for Photovoltaic Applications*, in proceedings 12th European Photovoltaic Solar Energy Conference (1994) 1743–1746

[47] T. Walter, D. Hariskos, R. Herberholz, V. Nadenau, R. Schäffler, and H. W. Schock, *On the Role of Oxidation for the Performance of Cu(In,Ga)(S,Se)$_2$ Polycrystalline Thin Film Solar Cells*, in proceedings 13th European Photovoltaic Solar Energy Conference (1995) 1999-2002

[48] K. L. Chopra and S. R. Das, *Thin Film Solar Cells*, Plenum Press (1983)

[49] A. W. Czanderna, F. J. Pern, *Encapsulation of PV Modules using Ethylene Vinyl Acetate Copolymer as a Pottant: A Critical Review*, Solar Energy Materials & Solar Cells **43** (1996) 101–181

[50] E. Cuddihy, C. Coulbert, A. Gupta, and R. Liang, *Electricity from Photovoltaic Solar Cells, Flat-Plate Solar Array Project, Final Report, Volume VII: Module Encapsulation*, JPL Publication **86-31**, Jet Propulsion Laboratory (1986)

[51] S. M. Sze, *Physics of Semiconductor Devices*, 2nd ed., John Wiley & Sons, Inc (1981)

[52] H. Håkansson and B. Fredlund, *A New Solar Simulation Facility for Calorimetric Measurements on Windows and Shading Devices*, in proceedings 5th Symposium on Building Physics in the Nordic Countries, Gothenburg (1999)

[53] R. Gay, M. Dietrich, C. Fredric, C. Jensen, K. Knapp, D. Tarrant, and D. Willett, *Efficiency and Process Improvements in $CuInSe_2$-Based Modules*, in proceedings 12th European Photovoltaic Solar Energy Conference (1994) 935–938

[54] M. Powalla and B. Dimmler, *Scaling Up Issues of CIGS Solar Cells*, Thin Solid Films **361–362** (2000) 540–546

[55] Y. Kuwano, T. Imai, M. Ohnishi, S. Nakano, *A Horizontal Cascade Type Amorphous Si Photovoltaic Cell Module (Integrated Type Amorphous Si Photovoltaic Cell Module*, in proceedings 14th IEEE Photovoltaic Specialists Conference (1980) 1408–1409

[56] J. Kessler, S. Wiedeman, L. Russell, T. Lommasson, S. Skibo, J. Fogleboch, T. Kloss, and R. R. Arya, *Progress in $Cu(In,Ga)Se_2$ Solar Cells and Submodules*, in proceedings 1st World Conference on Photovoltaic Solar Energy Conversion (1994) 206–209

[57] K. W. Mitchell, C. Eberspacher, J. H. Ermer, K. L. Pauls, and D. N. Pier, *$CuInSe_2$ Cells and Modules*, IEEE Trans. Elec. Dev. **37** (1990) 410–417

[58] J. Kessler, S. Wiedeman, L. Russell, J. Fogleboch, S. Skibo, R. Arya, and D. Carlson, *Front Contact Optimization for $Cu(In,Ga)Se_2$ (Sub)Modules*, in proceedings 25th IEEE Photovoltaic Specialists Conference (1996) 885–888

[59] M. Burgelman and A. Niemegeers, *Calculation of CIS and CdTe Module Efficiencies*, Solar Energy Materials & Solar Cells **51** (1998) 129–143

[60] J. Malmström, J. Wennerberg, and L. Stolt, *Influence of Ga on the Current Transport in $Cu(In,Ga)Se_2$ Thin Film Solar Cells*, to be published in proceedings 17th European Photovoltaic Solar Energy Conference (2001)

[61] W. N. Shafarman, R. Klenk, and B. E. MacCandless, *Device and Material Characterization of $Cu(InGa)Se_2$ Solar Cells with Increasing Band Gap*, J. Appl. Phys. **79** (1996) 7324–7328.

[62] M. Bodegård, O. Lundberg, J. Malmström, L. Stolt, and A. Rocket, *High Voltage $Cu(In,Ga)Se_2$ Devices with Ga-Profiling Fabricated using Co-Evaporation*, in proceedings 28th IEEE Photovoltaic Specialists Conference (2000) 450–453.

[63] H. W. Schock, U. Rau, T. Dullweber, G. Hanna, M. Balboul, T. Margorian-Friedelmeier, A. Jasenek, I. Kötschau, H. Kerber, and H. Wiesner, *High Efficiency, High Voltage Solar Cells by Band Gap and Defect Engineering in Cu(In,Ga)(S,Se)$_2$ Chalcopyrite Semiconductors*, in proceedings 16th European Photovoltaic Solar Energy Conference (2000) 304–308

[64] L. Spante, M. Andersson, B. Perers, P. Krohn, A. Helgesson, B. Karlsson, C. Setterwall, O. Gröndalen, M. Sunér, S. Holmström, L. Stolt, J. Wennerberg, M. Rönnelid, F. Kjellsson, L. Selhagen, P. Sandell, M. Forssander, B. Andersson, S. Ulvönäs, and M. A. Romero, *SOLEL 97-99 – Ett Branschgemensamt FoU-program Årsrapport 1997* (In Swedish), Elforsk AB, Elforsk rapport 98:2 (1998)

[65] J. Wennerberg and L. Stolt, *Technical and Physical Requirements on Solar Cells for Concentrating Systems* (in Swedish), Ångström Solar Center report ÅSC-011-CIGS-98 (1998)

[66] A. Meinel and M. Meinel, *Applied Solar Energy – An Introduction*, Addison-Wesley Publishing Company, Inc. (1976)

[67] W. T. Welford and R. Winston, *High Collection Nonimaging Optics*, Academic Press (1989)

[68] M. J. Carvalho, M. Collares-Pereira, J. M. Gordon, and A. Rabl, *Truncation of CPC Solar Collectors and its Effect on Energy Collection*, Solar Energy **35** (1985) 393–399

[69] M. Rönnelid, B. Perers, P. Krohn, L. Spante, and B. Karlsson, *Experimental Performance of a String Module in a CPC Reflector Cavity*, in proceedings 2nd World Conference on Photovoltaic Solar Energy Conversion (1998) 2264–2267

[70] B. Karlsson, P. Krohn, B. Perers, M. and Rönnelid, *Solceller med reflektorer – Resultat 1997* (In Swedish), Vattenfall Utveckling AB, Internal report UR 97/12 (1997)

[71] M. Rönnelid, B. Karlsson, P. Krohn, and J. Wennerberg, *Booster Reflectors for PV Modules in Sweden*, Progress in Photovoltaics: Research and Applications **8** (2000) 279–291

[72] M. A. Green, *Solar Cells – Operating Principles, Technology and System Applications*, University of New South Wales (1992)

[73] J. Wennerberg, and L. Stolt, *Performance Analysis of Standard Crystalline Silicon Solar Cells in Low-Concentrated Light*, internal PM within the framework of ELFORSK Projekt 2080 – SOLEL 97-99, Ångström Solar Center (1998)

[74] M. Brogren, M. Rönnelid, and B. Karlsson, *PV-Thermal Hybrid Low Concentrating CPC Module*, in proceedings 16th European Photovoltaic Solar Energy Conference (2000) 2121–2124

[75] M. Brogren, *Low-Concentrating Photovoltaic Systems with Parabolic Reflectors*, Licentiate Thesis, Uppsala University UPTEC 01 006 Lic (2001).

[76] M. Brogren, B. Karlsson, and H. Håkansson, *Design and Modelling of Low-Concentrating Photovoltaic Solar Energy Systems and Investigation of Irradiation Distribution on Modules in Such Systems*, to be published in proceedings 17th European Photovoltaic Solar Energy Conference (2001)

[77] *Thin-Film Terrestrial Photovoltaic (PV) modules – Design Qualification and Type Approval (CEI/IEC 1646:1996)*, International Electrotechnical Commission (IEC), First edition (1996)

[78] D. E. Tarrant, Al. R. Ramos, D. R. Willet, and R. R. Gay, *$CuInSe_2$ Module Environmental Durability*, in proceedings 22nd IEEE Photovoltaic Specialists Conference (1991) 553–556

[79] M. Powalla and B. Dimmler, *CIGS Solar Cells on the Way to Mass Production: Process Statistics of a 30 cm x 30 cm Module Line*, Solar Energy Materials & Solar Cells **67** (2001) 337–344

[80] J.-F. Guillemoles, L. Kronik, D. Cahen, U. Rau, A. Jasenek, and H.-W. Schock, *Stability Issues of $Cu(In,Ga)Se_2$-Based Solar Cells*, J. Phys. Chem. B **104** (2000) 4849–4862

[81] S. Roschier, *Development of Procedures for Performance Measurements and Lifetime Testing of Thin Film Photovoltaic Devices*, Thesis, Helsiniki University of Technology (2002)

[82] M. Powalla and B. Dimmler, *CIGS Solar Cells on the Way to Mass production: Process Statistics of a 30x30 cm Module Line*, Presented at the 11th International Photovoltaic Science and Engineering Conference (1999)

[83] F. H. Karg, D. Kohake, T. Nierhoff, B. Kühne, S. Grosser, and M. Ch. Lux-Steiner, *Performance of Grid Coupled PV-Arrays Based on CIS Solar Modules*, to be published in proceedings 17th European Photovoltaic Solar Energy Conference (2001)

[84] U. Rau, D. Braunger, R. Herberholz, H. W. Schock, J.-F. Guillemoles, L. Kronik, and D. Cahen, *Oxygenation and Air-Annealing Effects on the Properties of $Cu(In,Ga)Se_2$ Films and Devices*, J. Appl. Phys. **86** (1999) 497–505

[85] D. Hariskos, G. Bilger, D. Braunger, M. Ruckh, and H. W. Schock, *Investigations on the Mechanism of the Oxidation of $Cu(In,Ga)Se_2$*, Institute of Physics Conference Series No 152 (1998) 707–710

[86] M. Schmidt, D. Braunger, R. Schäffler, H. W. Schock, and U. Rau, *Influence of Damp Heat on the Electrical Properties of $Cu(In,Ga)Se_2$ Solar Cells*, Thin Solid Films **361–362** (2000) 283–287

[87] D. Braunger, D. Hariskos, and H. W. Schock, *Polycrystalline $Cu(In,Ga)Se_2$ Solar Cells*, in proceedings of the 2nd World Conference on Photovoltaic Solar Energy Conversion (1998) 511–514

[88] C. Heske, G. Richter, Z. Chen, R. Fink, E. Umbach, W. Riedl, and F. Karg, *Influence of Na and H_2O on the Surface Properties of $Cu(In,Ga)Se_2$ Thin Films*, J. Appl. Phys. **82** (1997) 2411–2420

[89] M. Powalla and B. Dimmler, *Process Development of High Performance CIGS Modules for Mass Production*, Thin Solid Films **387** (2001) 251–256

[90] A. Kylner, J. Lindgren, and L. Stolt, *Impurities in Chemical Bath Deposited CdS Films for Cu(In,Ga)Se_2 Solar Cells and Their Stability*, Journal of the Electrochemical Society **143** (1996) 2662–2669

[91] T. Nakada, M. Mizutani, Y. Hagiwara, and A. Kunioka, *High-Efficiency Cu(In,Ga)Se_2 Thin-Film Solar Cells with a CBD-ZnS Buffer Layer*, Solar Energy Materials & Solar Cells **67** (2001) 255–260

[92] K. Ramanathan, H. Wiesner, S. Asher, D. Niles, R. N. Bhattacharya, M. A. Contreras, and R. Noufi, *High-Efficiency Cu(In,Ga)Se_2 Thin Film Solar Cells Without Intermediate Buffer Layers*, in proceedings 2nd World Conference on Photovoltaic Solar Energy Conversion (1998) 477–482

[93] A. Goetzberger and C. Hebling, *Photovoltaic Materials, Past, Present, Future*, Solar Energy Materials & Solar Cells **62** (2000) 1–19

[94] H. W. Schock and R. Noufi, *CIGS-based Solar Cells for the Next Millennium*, Progress in Photovoltaics: Research and Applications **8** (2000) 151–160

[95] V. M. Fthenakis, S. C. Morris, P. D. Moskowitz, and D. L. Morgan, *Toxicity of Cadmium Telluride, Copper Indium Diselenide, and Copper Gallium Diselenide*, Progress in Photovoltaics: Research and Applications **7** (1999) 489–497

[96] A. Finke, A. Kriele, W. Thumm, D. Bieniek, and A. Kettrup, *Leaching Tests with Thin Film Solar Cells Based on Copper Indium Diselenide (CIS)*, Chemosphere **32** (1996) 1633–1641

[97] V. M. Fthenakis, *End-of-Life Management and Recycling of PV Modules*, Energy Policy **28** (2000) 1051–1058

[98] H.C. Lin and P. P. Hwang, *Acute and Chronic Effects of Indium Chloride ($InCl_3$) on Tilapia (Oreochromis mossambicus) Larvae*, Bulletin of Environmental Contamination and Toxicology **61** (1998) 123–128

[99] M. G. Dobbs, D. S. Cherry, and J. Cairns Jr., *Toxicity and Bioaccumulation of Selenium to a Three-Trophic Level Food Chain*, Environmental Toxicology and Chemistry **15** (1996) 340–347

[100] S. P. Canton and W. D. van Derveer, *Selenium Toxicity to Aquatic Life: an Argument for Sediment-Based Water Quality Criteria*, Environmental Toxicology and Chemistry **16** (1997) 1255–1259

[101] B. A. Andersson, *Material Constraints on Technology Evolution: The Case of Scarce Metals and Emerging Energy Technologies*, Thesis, Chalmers University of Technology and Gothenburg University (2001)